ARTICLE

https://doi.org/10.1590/2317-4889202120200046

BJGEO Brazilian Journal of Geology

The 1.88 Ga Uatumã Magmatism in the Serra dos Magalhães region: petrology and implications to the extension of the south-eastern edge of the Amazonian Craton

Ianna Ferreira de Lima[1,2], Ronaldo Pierosan[2,3]*, Márcia Aparecida de Sant'Ana Barros[2,3], Rogério Roque Rubert[2,3], Carlos Augusto Sommer[4], Diogo Isamu de Almeida Okuno[5]

Abstract

The Amazonian Craton (AC) is a Pre-Cambrian tectonic segment that extends over 4.3 × 10^5 km^2 at the northern portion of the South American Platform. Phanerozoic sedimentary basins cover most of the edges of the AC and sparse occurrences of Precambrian rocks may aid the definition of its extension. One of these occurrences is the volcano-plutonic rocks that outcrop in the Serra dos Magalhães region, which relates to the Uatumã Magmatism, an expressive Orosirian magmatic event that constitutes a Siliceous Large Igneous Province. Effusive rhyodacites and rhyolites comprise the volcanic unit and the plutonic counterpart consists of epizonal monzogranites. Whole-rock geochemistry indicates an A2-type granite affinity to all magmatic rocks. Contrasting signatures suggest a magmatic evolution from a single stratified magma chamber. U-Pb zircon crystallization ages are 1870 ± 11 Ma for the rhyodacites, 1879 ± 5 Ma for the monzogranites, and a slightly younger age of 1863 ± 14 Ma for the rhyolites. Interpretation of satellite and geophysical images allows the recognition of regional lineaments in the Parecis and Bananal basins that suggest the extension of the AC up to the Tucurui Fault in the eastern portion (Bananal Basin) and up to the Brasnorte High in the southern part (Parecis Basin).

KEYWORDS: volcano-plutonism; petrography; geochemistry; geochronology; Parecis Basin

INTRODUCTION

The Amazonian Craton (AC) is a Mesoarchean to Mesoproterozoic tectonic segment that extends over 4.3 × 10^5 km^2 at the northern portion of the South American Platform (Fig. 1). The north-western, western, and south-western limits make up the Andean Orogenic Belt, the southern border extends to the Neoproterozoic Paraguay Belt and the eastern and south-eastern edges prolong to the Neoproterozoic Araguaia Belt. Phanerozoic sedimentary basins cover most of the AC borders, as the Parecis, Chaco, Eastern Venezuela, and Bananal basins. The Phanerozoic Solimões-Amazonas Basin divide the Amazonian Craton into the Guyana Shield (northern part) and the Brazil Central Shield (southern portion).

The most expressive intraplate magmatic event of the AC, the Uatumã Magmatism, relates to the Uatumã Silicic Large Igneous Province (USLIP) (Klein *et al.* 2012) and consists of undeformed intermediate to acid volcanic rocks crosscut by cogenetic isotropic granitoids. This volcano-plutonism widespread from the northern portion of the AC to the south-eastern region. Well-known occurrences concentrate in the Pitinga Mining District, Presidente Figueiredo, and Erepecuru-Trombetas region (Guyana Shield), and in the Tapajós and Carajás mineral provinces, São Félix do Xingu and Confresa region (Brazil Central Shield) (Fig. 2). The volcanic rocks include effusive and hypabyssal andesites, dacites, trachytes, and rhyolites, beside ignimbrites, surge and ash-fall tuffs, and sedimentary volcanogenic rocks. The cogenetic granitoids comprise subvolcanic batholiths and stocks of coarse- to fine-grained monzogranites and syenogranites. Geochemical data indicate an I- to A-type affinity to the volcanic rocks and A-type to the granitoids. U-Pb crystallization ages range from 1.90 to 1.87 Ga (Dall'Agnol *et al.* 1999, Costi *et al.* 2000, Lamarão *et al.* 2002, Santos *et al.* 2004, Teixeira *et al.* 2005, Valério *et al.* 2009, Ferron *et al.* 2010, Pierosan *et al.* 2011, Barros *et al.* 2011, Fernandes *et al.* 2011, Rocha *et al.* 2012, Barreto *et al.* 2014, Tarelow Neto *et al.* 2017). Paleo- to Mesoproterozoic siliciclastic sedimentary rocks partially cover the USLIP and relate to the Gorotire Formation and Rio Fresco Group (Vasquez and Rosa-Costa 2008).

[1]Programa de Pós-Graduação em Geociências, Universidade Federal do Mato Grosso – Cuiabá (MT), Brazil. E-mail: iannafdelima@gmail.com

[2]Grupo de Pesquisa Magmatismo de Mato Grosso, Universidade Federal do Mato Grosso – Cuiabá (MT), Brazil. E-mails: ronaldo.pierosan@gmail.com, mapabarros@yahoo.com, rogrubert@yahoo.com.br

[3]Faculdade de Geociências, Universidade Federal do Mato Grosso – Cuiabá (MT), Brazil.

[4]Instituto de Geociências, Universidade Federal do Rio Grande do Sul – Porto Alegre (RS), Brazil. E-mails: casommer@sinos.net, diogo.geologia@gmail.com

[5]Graduação em Geologia, Universidade Federal do Mato Grosso – Cuiabá (MT), Brazil.

*Corresponding author.

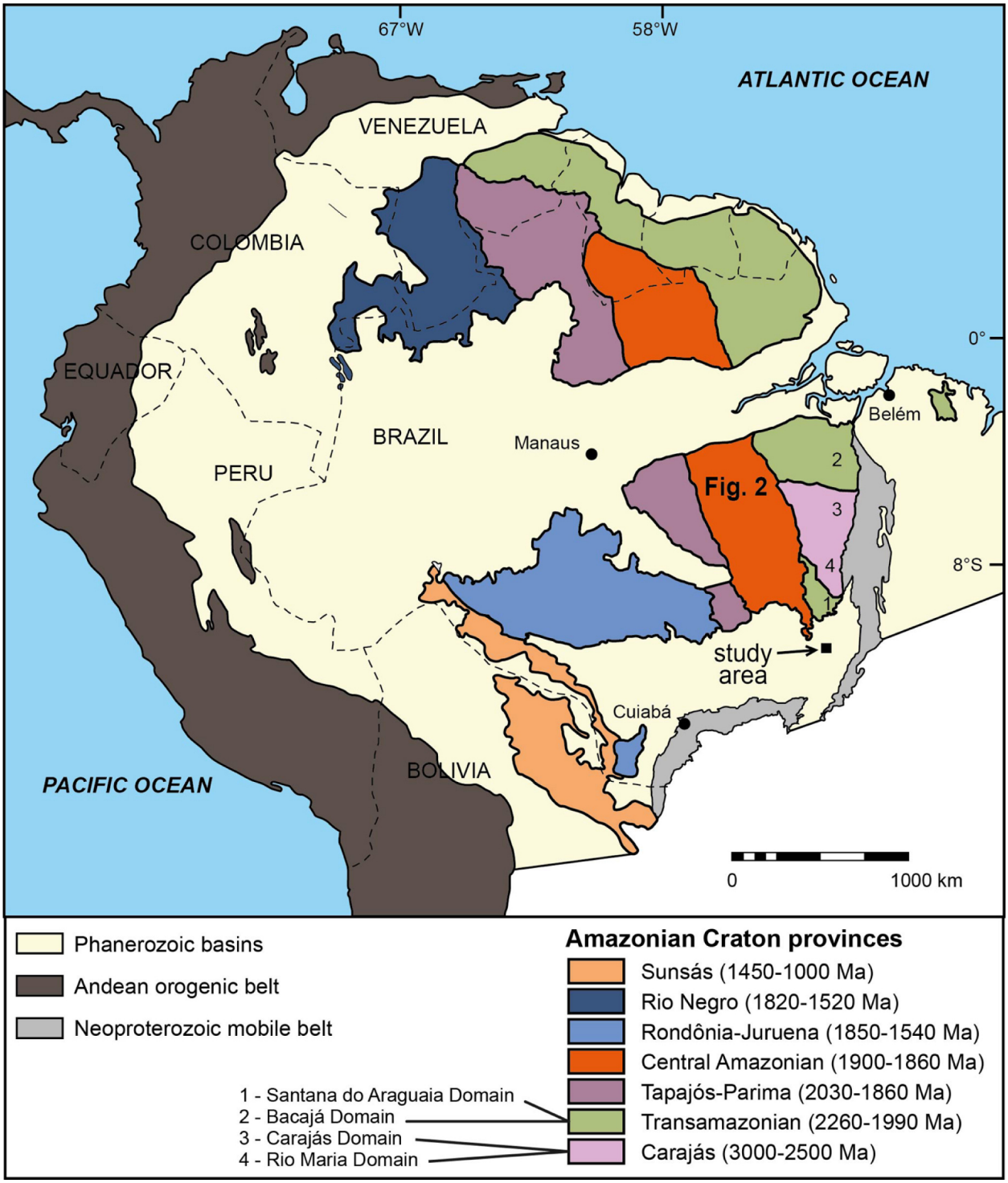

Figure 1. Sketch map of the Brazilian part of the Amazonian Craton and its geotectonic provinces (Vasquez and Rosa-Costa 2008).

The Phanerozoic sedimentary basins that cover most of the AC borders preclude an accurate definition of its limits. Thus, sparse occurrences of inliers amid the sedimentary basins play a key role to prescribe the extension of the AC edges. In this scenario, the present work deals with the geological investigation (field and petrographic information, whole-rock geochemistry, and U-Pb zircon isotopes) of the Serra dos Magalhães region that allows the determination of their petrological characteristics, aiming an appropriate correlation to the known occurrences within the AC. Moreover, this correlation supports meaningful considerations concerning the AC limits and its geotectonic implication to the South American Platform evolution.

GEOTECTONIC CONTEXT

The Tassinari and Macambira (1999) and Santos *et al.* (2000) models and further updates focus on the Brazilian part of the Amazonian Craton and describe, generically, the Archean nuclei followed by the successive magmatic arc and accretionary events whose ages decrease from the north-eastern to the south-western portion. Vasquez and Rosa-Costa

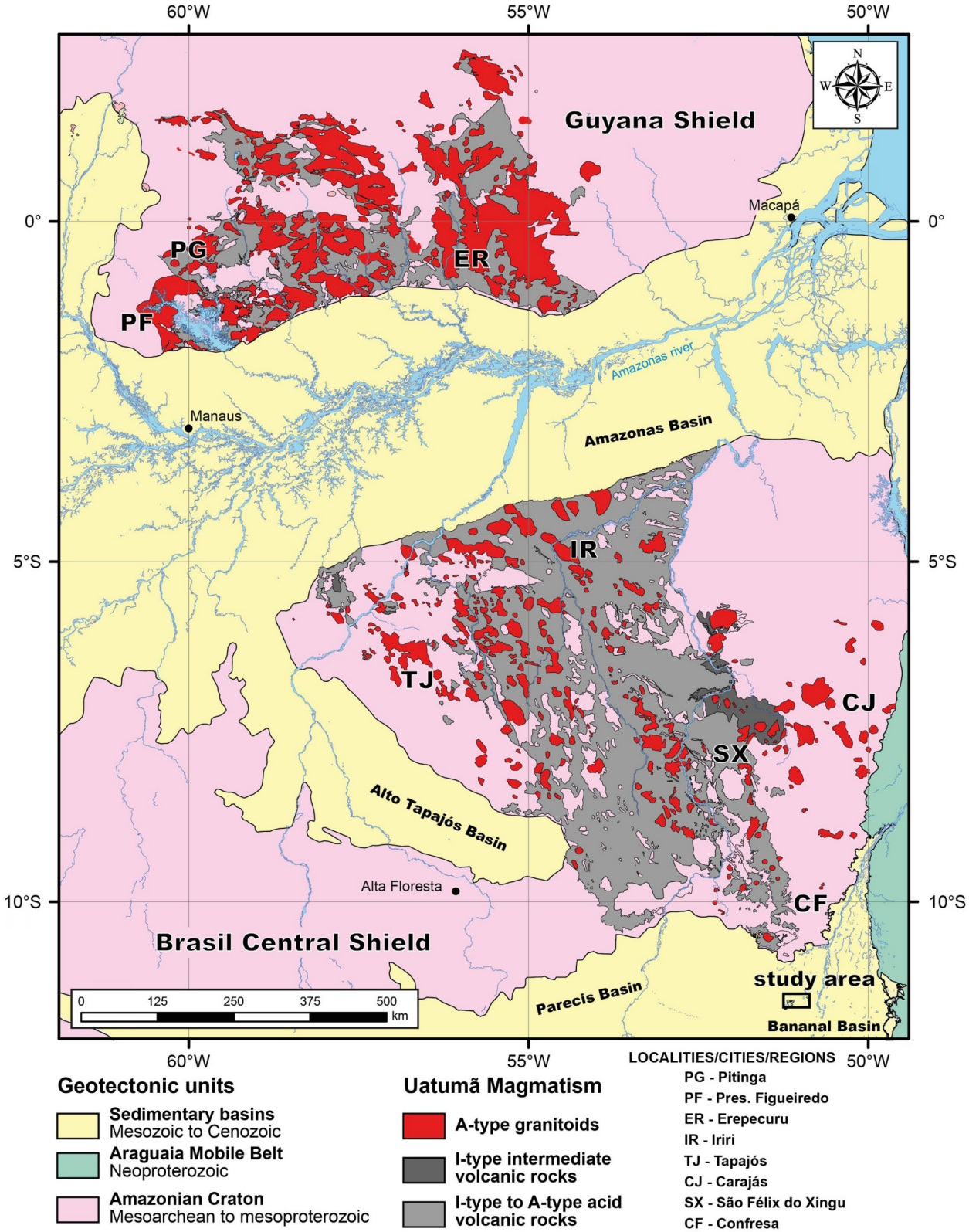

Source: adapted from Lacerda Filho *et al.* (2004), Reis *et al.* (2006) and Vasquez and Rosa-Costa (2008).
Figure 2. Spatial distribution of the Uatumã Silicic Large Igneous Province in the Amazonian Craton.

(2008) presented a model based on the Santos (2003) update that improves the description and interpretation of the geotectonic evolution of the central and south-eastern regions of the AC. This model defines new domains within some provinces and refines the limits of the south-eastern area.

The south-eastern portion of the Amazonian Craton, according to Vasquez and Rosa-Costa (2008), consists of Archean crustal segments included in the Carajás Province (Rio Maria and Carajás domains). The structural and metamorphic aspects of these domains indicate that the Transamazonian Cycle

(2.26 to 1.95 Ga) did not affect these rocks. On the other hand, the Archean crustal segments reworked by the Transamazonian Cycle and the Paleoproterozoic juvenile rocks generated during this orogenic cycle integrate the Transamazonian Province. The Transamazonian Province is divided into the Amapá Block and the Bacajá, Carecuru, and Paru domains, in the eastern part, and in the Santana do Araguaia Domain in the south-eastern portion.

The Santana do Araguaia Domain includes Neoarchean metavolcanossedimentary sequences and granite-gneiss-migmatite associations, and Rhyacian pre-collisional granitoids. Post-tectonic Orosirian granitoids crosscut the older units and intracratonic sedimentary basins cover part of the domain. The Neoarchean metavolcanossedimentary sequences relate to greenstone belts, from which Pb-Pb zircon data of detrital grains show a youngest age of 2833 ± 7 (Monteiro *et al.* 2004), interpreted as the maximum sedimentation age. The Santana do Araguaia Complex and the Rio Campo Alegre Orthogneiss comprise the Archean granite-gneiss-migmatite associations and show Pb-Pb zircon protolith ages from 3066 ± 3 to 2828 ± 21 Ma (Alves *et al.* 2010, Vasquez and Rosa-Costa 2008, Corrêa and Macambira 2014, Ribeiro and Alves 2017). The Pb-Pb zircon crystallization age of the Rio Dezoito Tonalite of 2187 ± 28 Ma (Vasquez and Rosa-Costa 2008) and the structural and lithological aspects of this unit suggest that the Rhyacian granitoids relate to the pre-collisional stage of the Transamazonian Cycle. Post-collisional magmatism relates to the volcano-plutonic association of the Jarinã Formation and the Vila Rica Intrusive Suite, respectively (Lacerda Filho *et al.* 2004, Alves *et al.* 2010, Ribeiro and Alves 2017). The crystallization ages of the Jarinã Formation vary from 2009 ± 9 to 1987 ± 14 Ma and of the Vila Rica Intrusive Suite from 1995 ± 14 to 1968 ± 2 Ma (Padilha *et al.* 2007, Barros *et al.* 2008, Alves *et al.* 2010, Ribeiro and Alves 2017, Braga *et al.* 2020).

The Central Amazonian Province represents one of the most poorly known areas of the AC, mainly due to the dense rainforest cover and several biological and indigenous reserves. The basement rocks consist of schists, para- and orthogneisses, and migmatitic gneisses with leucossome ages from 2155 ± 8 to 1983 ± 5 Ma, protolith age of 1990 ± 3 Ma, and inherited age of 2160 ± 8 Ma (Vasquez *et al.* 2019). The volcano-plutonic event of the USLIP concentrates in the Central Amazonian Province and spread throughout the Tapajós-Parima, Transamazonian, and Carajás provinces. In the south-eastern region of the AC, the volcanic rocks comprise intermediate to acid effusive and pyroclastic lithotypes of I- to A-type affinity and crystallization from 1896 ± 5 to 1865 ± 5 Ma (Rocha *et al.* 2012, Tarelow Neto *et al.* 2017, Vasquez and Rosa-Costa 2008). The Rio Dourado Intrusive Suite groups the granitoids in the south-eastern of the AC, which essentially show A-type signature and ages that range from 1891 ± 3 to 1864 ± 5 Ma (Alves *et al.* 2010, Barros *et al.* 2005, 2006, 2008, 2011, Pinho *et al.* 2004).

The Tapajós-Parima Province occurs in the central portion of the AC, as defined by Santos *et al.* (2000) and Santos *et al.* (2004), and includes successive magmatic arcs developed between 2.10 and 1.87 Ga. These arcs associate to metavolcanossedimentary sequences of the Jacareacanga Group with ages of deposition around 2.1 Ga and metamorphic rocks of the Cuiú-Cuiú Complex of U-Pb zircon protolith ages from 2033 ± 7 to 2005 ± 7 Ma (Klein *et al.* 2001, Santos *et al.* 2001, Vasquez *et al.* 2013). An isotropic volcano-plutonic association (Vila Riozinho Formation and correlated volcanic rocks and Creporizão Intrusive Suite and correlated granitoids) shows shoshonitic to I-type signatures, respectively, and U-Pb zircon crystallization ages from 2002 ± 4 to 1955 ± 4 Ma (Lamarão *et al.* 2002, 2008, Santos *et al.* 2001, Santos *et al.* 2004, Vasquez *et al.* 2000, 2013, Cassini *et al.* 2020).

Extensive sedimentary rocks cover older units of the Carajás, Transamazonian, Tapajós-Parima, and Central Amazonian provinces. In the south-eastern portion, they are related to the Gorotire Formation and Rio Fresco Group (Vasquez and Rosa-Costa 2008). Cunha *et al.* (1981) indicate a maximum sedimentation age of 1.88 Ga for the sedimentary rocks of the Gorotire Formation. However, Alves *et al.* (2010) assume, based on stromatolites levels, a deposition period between 1.96 and 1.88 Ga, and group the sedimentary rocks in the Cubencranquém Formation. The lack of provenance studies, mainly of U-Pb zircon data, hinder a better definition of these sedimentary rocks.

The Mesozoic sedimentary Parecis Basin covers the central-south edge of the Amazonian Craton and consists of an Upper Cretaceous sequence, named Rio Tapirapé Formation by Rubert *et al.* (2017, 2019), which comprises one restrict intracontinental lacustrine and deltaic-fluvial sequence. The bottom layer records a chemical and low energy clastic sedimentation of mudstones, marls and limestones, siltstones, and fine sandstones, that relates to a lacustre and marine environment in a context of fast initial subsidence and low sedimentation rate in the base of the package. Laminated siltstones and massive to stratified sandstones and conglomerates overlay the bottom package and are comprised of a prodelta and deltaic progradation environment that become dominant to the top of the package. Massive to laminated sandstones and mudstones compose the top of the sequence and relate to fluvial, alluvial plain, and aeolian deposition.

The south-eastern border of the Amazonian Craton is covered by the Parecis Basin, composed by Cenozoic packages of Paleogene of the Ronuro Formation that records the reworking of the Cretaceous sedimentary sequence and consists of packages of unconsolidated sediments as silts, sands, and gravel interbedded with laterite levels (Alves *et al.* 2010). The Neogene Araguaia Formation (Barbosa *et al.* 1966) belongs to the Bananal Basin, which also covers the south-eastern border of the Amazonian Craton, and comprises partially unconsolidated conglomerates at the bottom, covered by sands, silts, and clays of low selection and related to terraces and abandoned channels of fluvial systems. Valente (2007) relates this unit to the Pleistocene period.

MATERIALS AND METHODS

Seventeen outcrops were identified and described in the Serra dos Magalhães region during two field trips. Representative samples of the different lithotypes were collected for petrographic,

geochemical, and geochronological studies. The thin section preparation and petrographic studies followed conventional procedures and were performed at the Geoscience Faculty labs of *Universidade Federal do Mato Grosso* (FAGEO/UFMT), Brazil.

Ten samples were crushed and powdered in a jaw crusher and disc mill at the FAGEO/UFMT. The commercial lab Acmelab performed the geochemical analysis by Inductively Coupled Plasma-Atomic Emission Spectrometry (ICP-AES) for major and minor elements and Inductively Coupled Plasma-Mass Spectrometry (ICP-MS) for trace elements, including rare earth elements (REE). The quality control report of the Acmelab included two analyses of the SO-18 standard, one blank, and two sample duplicates. All results are within the expected error. Temperature calculations were run through the model of Hanchar and Watson (2003). Rheological data were calculated according to the Giordano *et al.* (2008) model. Best-fit of viscosity and glass transition temperature data *versus* estimated water content were run through nonlinear curve by an exponential decay with 2 degrees of freedom.

Three samples were crushed and sieved to 250, 210, 177, 125, 90, and 63 mesh fractions to select zircon grains for the U-Pb geochronological analysis. Fractions of 90 and 63 mesh were selected for magnetic and density zircon separation. Around 100 zircon grains were hand-picked from each sample. Geochronological analyses of samples DI-14a and DI-17a were performed at the Geochronological Research Centre of *Universidade de São Paulo* (CPGeo/USP), Brazil, where the isotopic U-Pb ratios were obtained through LA-ICP-MS using a Neptune instrument from Thermo Finnigan. The instrument's parameters consisted of a ratio frequency of 1,100 W, Ar gas flow rates of 15 L/min (cool), 0.7 L/min (auxiliary), and 0.6 L/min (sample). The excimer laser had an energy of 6 mJ at a repetition rate of 6 Hz and a spot size of 32 μm. Collectors positions consisted of IC3: ^{202}Hg, IC4: ^{204}Pb, L4: ^{206}Pb, IC6: ^{207}Pb, L3: ^{208}Pb, H2: ^{232}Th, H4: ^{238}U, and C: virtual mass. The U-Pb analysis sequence was of 2 blanks, 2 NIST standard glass, 3 external standards (GJ1), 13 unknown samples (zircon), 2 NIST standard glass, 2 external standards (GJ1) and 2 blanks. GJ1 external standard has a reference age of 608.5 ± 0.4 Ma (Jackson *et al.* 2004) and yielded an age of 602.2 ± 0.9 Ma. Two sequences were performed for each sample, totalizing 26 analyzed zircon grains. Each zircon grain was analyzed by 40 cycles of 1s/cycle. ^{202}Hg was used to correct the ^{204}Hg interference in ^{204}Pb. The common Pb was subsequently corrected using the ^{204}Pb method with a composition taken from the model of Stacey and Kramers (1975). The sample DI-10a was analyzed by the ionic microprobe SHRIMP II of the geochronology lab of the Curtin University, Perth, Australia. The analytical methodology followed the parameters described by Williams (1998). The following masses were analyzed in the zircons: $^{196}Zr_2O$, ^{204}Pb, background, ^{206}Pb, ^{207}Pb, ^{208}Pb, ^{238}U, ^{248}ThO, ^{254}UO. Calibration was performed using the M257 zircon reference material (561.3 Ma). Common lead correction was run by counting the ^{204}Pb. The international reference material BR-266, which ^{206}Pb/^{238}U age is of 559 Ma, was used for calculation correction. The diagrams and ages were calculated using the Isoplot 4 software by Ludwig (2012).

RESULTS

Field aspects and petrography

The study area consists of an inlier of volcanic (Iriri Group), granitic (Rio Dourado Intrusive Suite), and sedimentary rocks (Gorotire Formation), surrounded and partially covered by recent alluvial deposits and terraces (Araguaia Formation) (Fig. 3). Volcanic rocks outcrop in the western portion of the study area and form the geomorphological highs of the Serra dos Magalhães. Granitic and sedimentary rocks outcrop at around 25 km from the Serra dos Magalhães region, in the northeast region of the study area. The basement of the volcanic and sedimentary rocks and the country rocks of the granitoids do not outcrop. Alluvial deposits and terraces cover most of the study area.

Outcrops of all units are rare and sparse and consist of boulders, blocks, and subordinate flooring outcrop of fresh to weakly weathered volcanic and granitic rocks and strongly weathered sedimentary rocks amid regolithic soils and alluvial deposits. The limits of the volcanic rocks were identified by relief and satellite images analysis allied to the occurrence of outcrops of the alluvial deposits. The limits of the granitic body were kept as those established by Cunha *et al.* (1981) due to the lack of continuous outcrops or relief and satellite image features that allowed a better delimitation. Figure 3 presents the geological map generated by this work and the geological section from its interpretation.

Based on field and petrographic observations, three volcanic lithotypes, one granitic, and one sedimentary were recognized. Volcanic rocks comprise massive rhyodacite, massive rhyolite, and flow-banded rhyolite. The granitoid consists of porphyritic monzogranite and the sedimentary rocks are a polymictic conglomerate.

Massive rhyodacites (Iriri Group)

The massive rhyodacites are of greenish dark grey color, holocrystalline, porphyritic with around 30 modal% of alkali-feldspar, plagioclase, quartz, and hornblende phenocrysts in micro- to cryptocrystalline aphanitic and quartz-feldspathic groundmass (Figs. 4A and 4B). Subhedral to euhedral phenocrysts are dominant and crystal fragments are rare.

Plagioclase is the most abundant phenocryst, comprises around 50 modal%, and is subhedral to euhedral, with sizes from 0.3 to 2.0 mm (Fig. 4C). Alkali-feldspar (around 10 modal%) shows subhedral to euhedral habit and size from 0.5 to 2.5 mm. Carlsbad twinning occurs locally. Quartz sums 20% of the phenocrysts, ranges from 0.2 to 3.5 mm, and is subhedral to euhedral with bipyramidal forms and common embayments. Hornblende is subhedral to anhedral, comprises around 20% of the phenocrysts and ranges from 0.3 to 1.5 mm (Fig. 4D). The pleochroism varies from medium green to light brown color. Pseudomorphs of chlorite+epidote partially to completely replace the hornblende. Apatite, zircon, and opaque minerals are present in the groundmass as accessory minerals. Subsolidus alteration minerals are subordinate, distribute pervasively through the groundmass, and mostly replace phenocrysts. They consist of chlorite and epidote as replacement

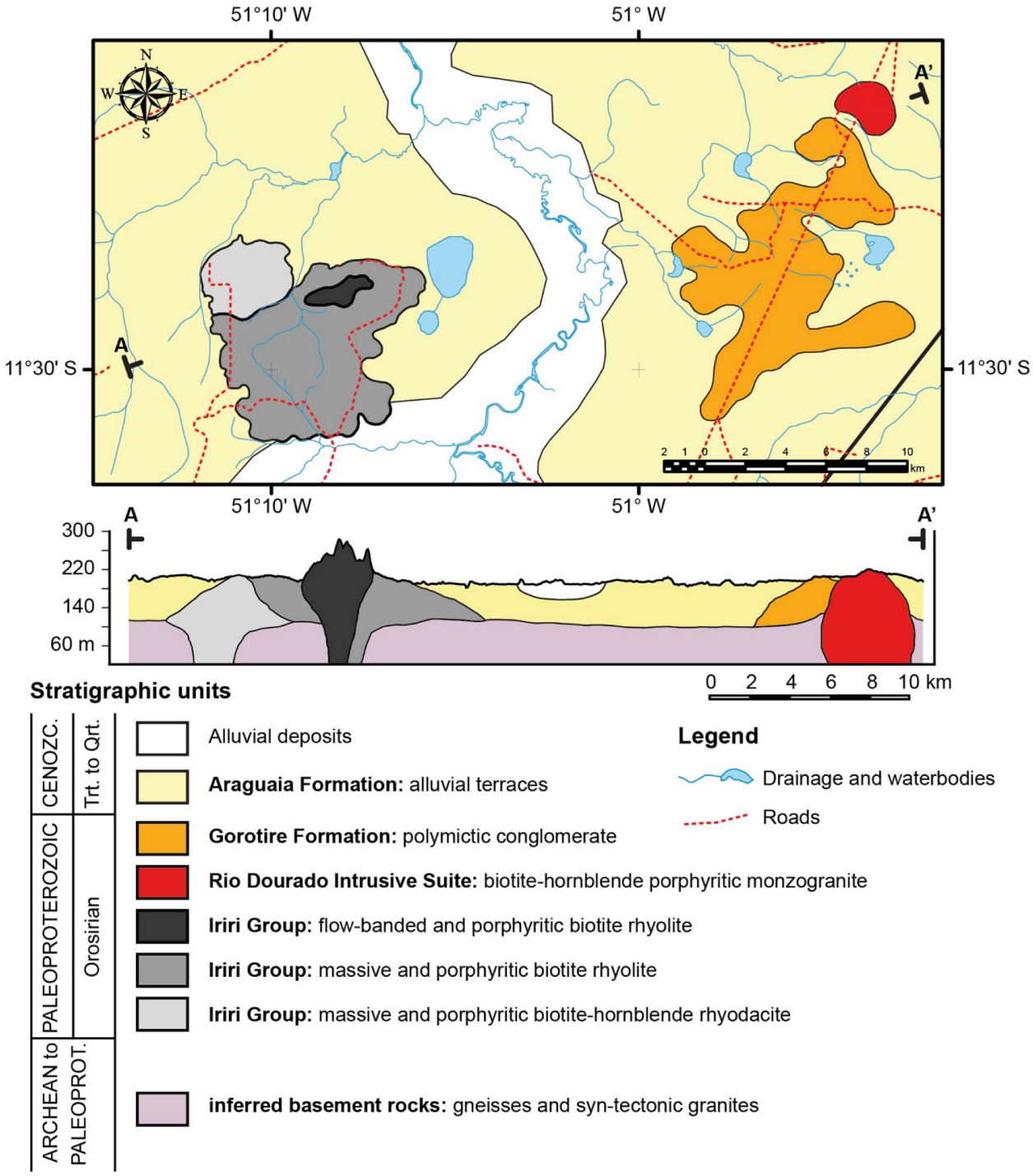

Figure 3. Geological map and the geological section of the Serra dos Magalhães region.

of hornblende and white mica and calcite as alteration of plagioclase.

Massive rhyolites (Iriri Group)

Massive rhyolites are of light grey to light red color, holocrystalline, and porphyritic with around 25 modal percent of alkali-feldspar, quartz, and plagioclase phenocrysts in crypto- to microcrystalline aphanitic and quartz-feldspathic groundmass (Figs. 5A and 5B). Phenocrysts are dominantly subhedral to euhedral and crystal fragments are subordinate.

Alkali-feldspar phenocrysts are subhedral, of prismatic to round habit and with 0.2 to 4.0 mm. They show the common film to chessboard perthites (Fig. 5C) and less Carlsbad twinning and compose around 45% of the phenocrysts. Quartz phenocrysts are anhedral to subhedral of short prism to rounded forms with recurrent embayments. They vary from 0.2 to 3.5 mm and comprise around 45% of the phenocrysts. Plagioclase consists of subhedral to euhedral prismatic phenocrysts with characteristic polysynthetic twinning, varying from 0.3 to 2.0 mm and amounts of 10%. A jigsaw texture occurs locally and consists of fragments of quartz and feldspars phenocrysts with microscopic dislocation of the fragments filled by a thin portion of groundmass (Fig. 5D). This feature frequently associates with the recurrent embayments of

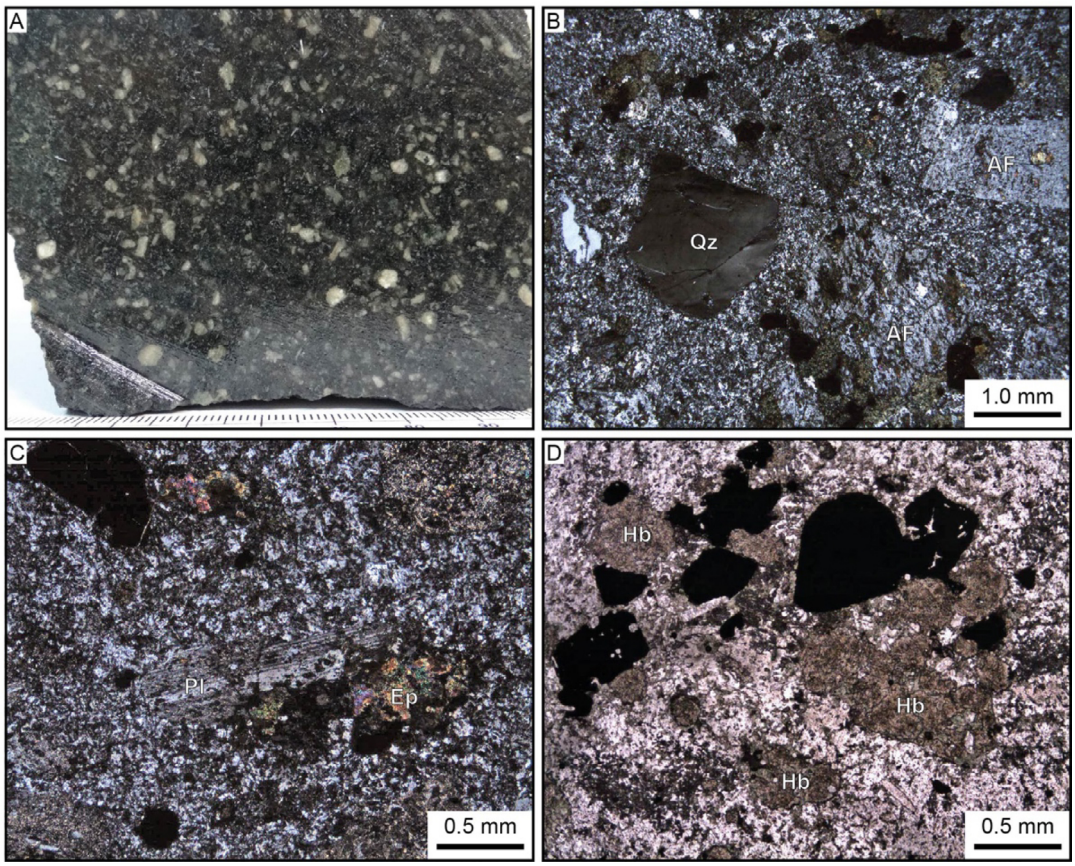

Figure 4. Petrographic features of the massive rhyodacites of the Iriri Group in the Serra dos Magalhães region. (A) Macroscopic aspect. (B) Porphyritic texture. (C) Plagioclase in an aphanitic groundmass. (D) Hornblende and opaque minerals in an aphanitic groundmass.

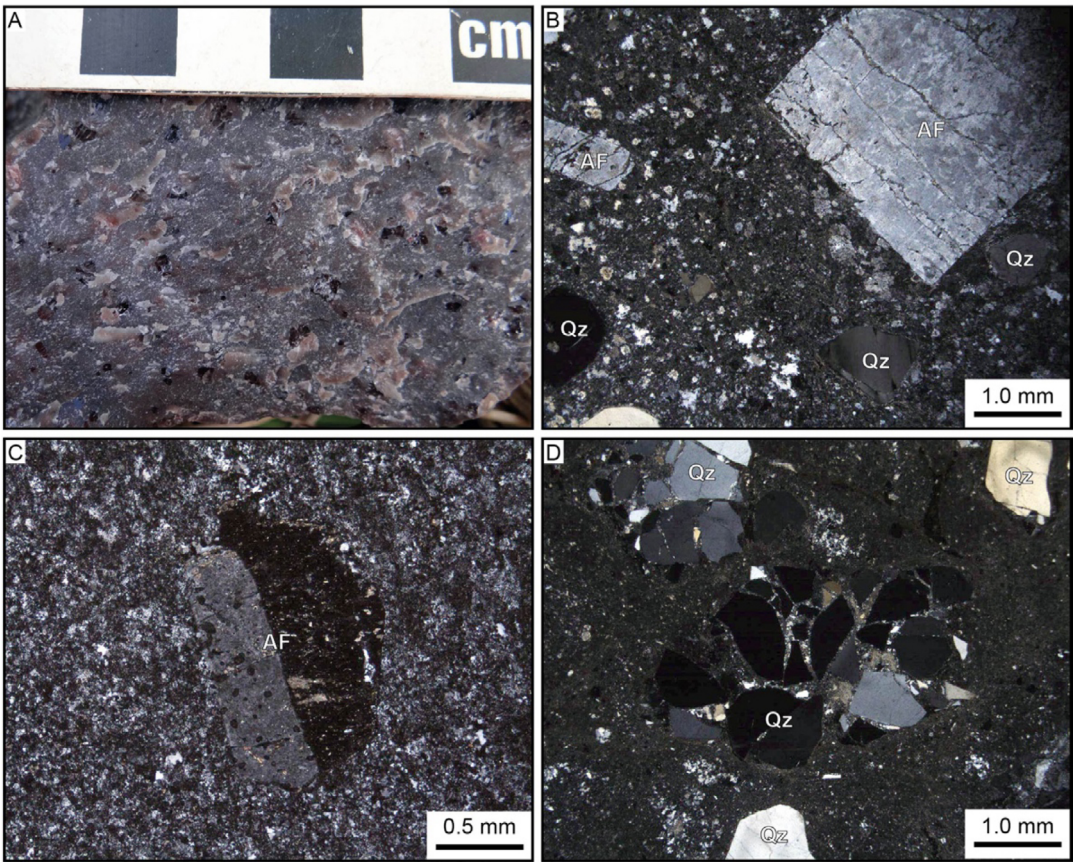

Figure 5. Petrographic features of the massive rhyolites of the Iriri Group in the Serra dos Magalhães region. (A) Macroscopic aspect. (B) Porphyritic texture with euhedral and perthitic alkali-feldspar phenocryst. (C) Twinned alkali-feldspar phenocryst in an aphanitic groundmass. (D) The jigsaw-fit texture of quartz phenocrysts.

the quartz phenocrysts. Accessory minerals are comprised of common subhedral to euhedral prismatic zircon, frequently metamict, anhedral opaque minerals, and rare subhedral prismatic apatite. Subsolidus minerals are subordinate, distribute in the groundmass, and replace the phenocrysts. White mica is the main alteration of plagioclase along with calcite, epidote partially replaces the alkali-feldspar and opaque minerals pervasively distribute throughout the groundmass.

Flow-banded rhyolites (Iriri Group)

The flow-banded rhyolites are of grey to dark grey color, hypocrystalline, porphyritic and contain around 10 modal% of alkali-feldspar, quartz, and plagioclase phenocrysts in a cryptocrystalline aphanitic to glassy groundmass (Figs. 6A and 6B). Phenocrysts are subhedral to euhedral and fragmented terminations are common.

Quartz phenocrysts are subhedral to euhedral with bipyramidal forms and common embayments. They vary from 0.2 to 1.5 mm and comprise around 50% of the phenocrysts. Alkali-feldspar phenocrysts are dominantly subhedral, show Carlsbad twinning in some crystals, compose around 45% of the phenocrysts, and range from 0.5 to 2.0 mm. Plagioclase is euhedral to subhedral, from 0.5 to 1.8 mm, and consists of less than 5.0% of the phenocrysts. Subhedral prismatic zircon is the only accessory mineral observed. Groundmass displays a prominent flow foliation marked by the regular alternation of millimetric layers of different crystallinity degree since glassy to crypto- and microcrystalline. Flow foliation is a dominantly planar structure and locally depicts open to convolute folds (Fig. 6C), sometimes outlining phenocrysts. The glassy portion of the groundmass presents isolated and aggregated spherulites of millimetric size with radial morphology of quartz and feldspars microlites and crystallites (Fig. 6D). Micropoikilitic texture is subordinate and consists of acicular microlites of quartz enclosing granular microlites of feldspars. Calcite, epidote, and white mica are rare, sparsely distribute throughout the groundmass, and partially replace feldspars.

Porphyritic monzogranite (Rio Dourado Intrusive Suite)

The porphyritic monzogranite is of light grey color, isotropic, and shows a medium- to coarse-grained inequigranular phaneritic texture with alkali-feldspar megacrysts up to 3.5 cm (Fig. 7A). The essential mineralogy consists of alkali-feldspar (40 modal%), plagioclase (25 modal%), quartz (20 modal%), hornblende (8.0 modal%), and biotite (5.0 modal%).

Alkali-feldspar is subhedral to rarely euhedral and usually varies from 1.5 to 4.0 mm. Megacrysts of alkali-feldspar randomly distribute through the rock and range from 0.7 to 3.5 cm. The poikilitic texture is common and consists of < 1.0 mm crystals inclusions of euhedral to subhedral plagioclase, hornblende and biotite, and anhedral quartz, within the alkali-feldspar grains (Fig. 7B). Perthitic intergrowths are subordinate and comprise thin films of exsolved albite. Rapakivi texture occurs locally and characterizes as a millimetric sized mantle of plagioclase enveloping the alkali-feldspar crystals. Plagioclase

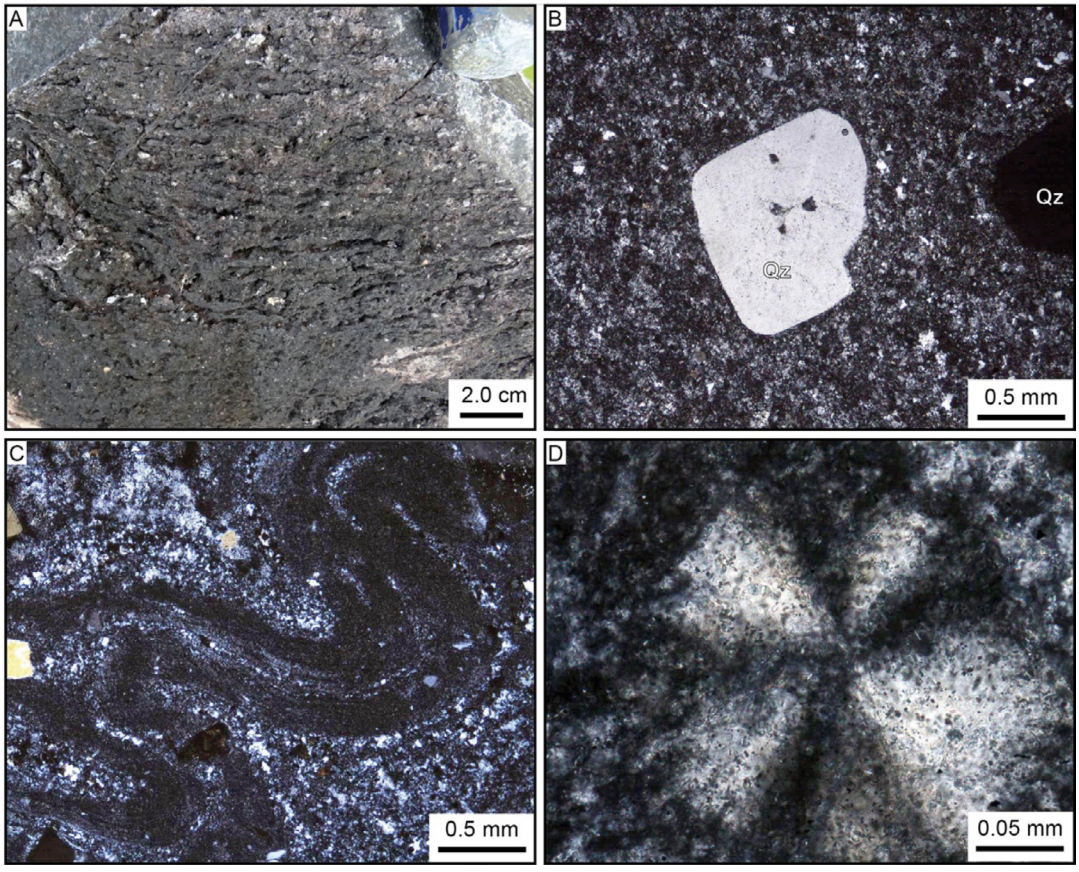

Figure 6. Petrographic features of the flow-banded rhyolites of the Iriri Group in the Serra dos Magalhães region. (A) Flow foliation in outcrop. (B) Euhedral and embayed quartz phenocryst. (C) The convolute fold of flow foliation. (D) Spherulite.

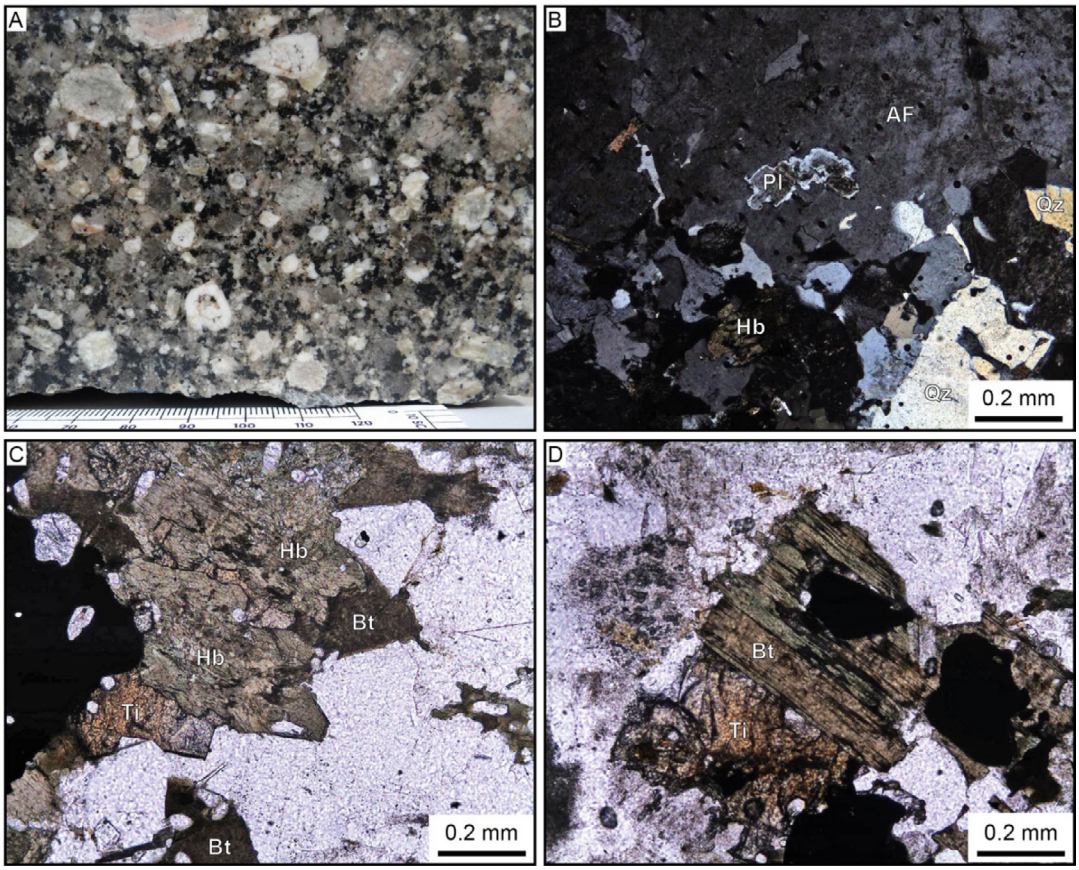

Figure 7. Petrographic features of the porphyritic monzogranite of the Rio Dourado Intrusive Suite in the Serra dos Magalhães region. (A) Macroscopic aspect. (B) Subhedral plagioclase inclusion within alkali-feldspar. (C) A mafic aggregate of hornblende, biotite, titanite, and opaque minerals. (D) Biotite partially replaced by chlorite.

crystals are subhedral to euhedral of tabular forms, with characteristic polysynthetic twinning and size between 0.5 and 4.0 mm. Quartz is dominantly anhedral interstitial and varies from 0.25 to 2.5 mm. Hornblende show light to dark green pleochroism, subhedral forms, and range from 0.3 to 2.0 mm (Fig. 7C). Biotite shows a characteristic lamellar habit with subhedral to euhedral forms and width from 0.4 to 2.0 mm (Fig. 7D). Biotite pleochroism varies from light green to brown color. Mafic and accessory minerals, mainly opaque minerals, frequently occur as aggregates of up to 1.0 cm. Accessory minerals consist of anhedral titanite, subhedral to anhedral opaque minerals, subhedral prismatic zircon, and subhedral to euhedral apatite with a short prism to acicular habit. Subsolidus phases are scarce and comprise of chlorite, which locally replaces hornblende and biotite crystals as pseudomorphs, and white mica and rare epidote that usually associates to feldspars.

WHOLE-ROCK GEOCHEMISTRY

Whole-rock geochemical data of three massive rhyodacites, four massive rhyolites, one flow-banded rhyolite, and two porphyritic monzogranites are reported in Table 1. SiO_2 content of the massive rhyodacites is around 65wt. % and are similar to the silica content of the porphyritic monzogranites (65.62 and 68.55wt. %), whereas the rhyolites show higher values, from 74.91 to 81.53wt. %. Binary diagrams of major, minor, and trace elements demonstrate higher values of Al_2O_3, FeO^t, MgO, CaO, TiO_2, P_2O_5, Ba, Sr, Zr, and Eu in the massive rhyodacites and the porphyritic monzogranite compared with the flow-banded and the massive rhyolites. Exceptions are the Ba, Zr, and Eu content of the flow-banded rhyolites that are higher than the massive ones. K_2O, Rb, Nb, Th, and Yb are higher in the rhyolites than in other lithotypes, except the Th content of the flow-banded rhyolite (Fig. 8). The element distribution in the binary diagrams indicates similarities between massive rhyodacites and porphyritic monzogranite that contrast to the rhyolites. There are no positive or negative correlations among the different lithotypes. These features suggest that they preferably evolved from distinct batches of magma rather than by crystal fractional crystallization and/or magma mixing processes.

The spidergram of major and trace elements normalized to the Thompson (1982) chondrite demonstrates a decrease in elements content with the compatibility increase, from Rb to Yb. All lithotypes show negative anomalies of Ba, Nb, Ta, Sr, P, and Ti. However, Sr, P, and Ti negative anomalies are smaller in the massive rhyodacites and porphyritic monzogranite than in the rhyolites (Fig. 9A). The spidergram of REE normalized to the Boynton (1984) chondrite illustrates the higher REE contents, except Eu, of the flow-banded and massive rhyolites, compared with the massive rhyodacites and the porphyritic monzogranites. Eu negative anomaly is strong in

Table 1. Geochemical data of major, minor (wt.%), and trace elements (ppm) of the volcanic rocks of the Iriri Group and the granitoids of the Rio Dourado Intrusive Suite.

Unit	IG	IG	IG	IG	IG	IG	IG	IG	RDIS	RDIS
Sample	DI10a	DI11a	DI12a	DI04a	DI03a	DI14a	DI02a	DI01a	DI16a	DI17a
Litology	RD	RD	RD	FRI	MRI	MRI	MRI	MRI	PMZ	PMZ
SiO_2	65.40	65.42	65.95	74.91	75.56	76.75	77.27	81.53	65.62	68.55
Al_2O_3	13.77	13.79	13.75	12.13	12.18	11.79	11.60	9.22	14.22	13.54
Fe_2O_3t	6.28	6.24	6.24	2.17	1.67	1.50	1.36	1.31	4.97	3.96
FeOt	5.65	5.61	5.61	1.95	1.50	1.35	1.22	1.18	4.47	3.56
MnO	0.12	0.11	0.11	0.05	0.02	0.04	0.02	0.03	0.09	0.07
MgO	1.22	1.55	1.60	0.01	0.07	0.10	0.09	0.10	1.04	0.81
CaO	3.28	2.89	2.81	0.89	0.27	0.37	0.56	0.29	2.68	2.19
Na_2O	2.61	2.68	2.67	3.12	2.01	2.48	2.60	1.30	3.47	3.32
K_2O	3.98	3.76	3.87	5.19	5.90	5.56	5.27	4.99	4.38	4.58
TiO_2	0.97	0.96	0.97	0.15	0.16	0.13	0.13	0.12	0.80	0.64
P_2O_5	0.22	0.24	0.24	0.01	<0.01	0.02	0.01	<0.01	0.24	0.19
P.F.	1.80	2.00	1.50	1.00	1.90	1.10	0.90	0.90	2.10	1.80
Total	99.71	99.70	99.72	99.65	99.75	99.79	99.78	99.80	99.60	99.66
Ga	19.30	18.70	17.80	20.00	17.50	18.50	18.10	13.10	19.10	17.20
Hf	7.20	8.00	7.20	9.60	7.80	6.90	6.50	6.10	8.70	7.60
Nb	13.40	12.60	12.30	16.60	18.60	18.80	19.00	17.50	12.30	12.20
Rb	191.50	170.30	168.00	220.80	255.40	262.70	240.00	230.40	156.90	174.00
Sr	239.60	216.00	221.90	97.40	67.50	31.30	40.80	23.00	300.00	239.10
Ta	1.10	1.00	1.00	1.40	1.60	1.90	1.90	1.60	0.90	1.10
Th	19.50	19.10	18.10	20.40	25.80	27.90	24.70	23.10	15.70	19.10
U	3.90	3.90	3.90	5.10	5.80	5.50	5.70	4.90	2.80	3.80
V	81.00	79.00	79.00	<8	<8	<8	<8	<8	46.00	40.00
W	318.9	250.8	254.9	556.9	519.0	518.7	574.7	623.9	465.4	539.4
Zr	269.5	314.3	266.9	301.0	230.5	198.6	198.6	176.7	341.3	287.7
Y	38.60	38.50	38.30	66.00	61.30	59.30	69.80	58.30	38.20	37.50
Ba	966.0	957.0	888.0	1455.0	632.0	316.0	360.0	302.0	1658.0	1168.0
La	56.20	51.50	53.70	69.10	92.00	87.50	96.10	77.40	57.70	63.00
Ce	110.1	100.9	102.4	134.0	176.4	170.5	182.0	145.1	112.4	119.0
Pr	12.29	11.71	11.61	15.71	20.33	19.13	20.95	16.67	13.27	13.43
Nd	46.90	44.30	43.60	60.60	74.20	72.20	77.70	60.60	49.70	49.70
Sm	8.64	8.75	8.29	12.00	14.09	12.99	14.48	11.43	8.82	8.39
Eu	1.83	1.70	1.75	2.03	1.05	0.70	0.81	0.61	2.11	1.77
Gd	8.36	8.05	7.87	12.10	12.28	12.59	13.63	10.82	8.01	7.75
Tb	1.21	1.23	1.21	1.92	1.93	1.92	2.13	1.66	1.19	1.18
Dy	6.45	6.78	6.45	11.18	10.94	11.22	12.28	9.80	6.78	6.61
Ho	1.34	1.32	1.35	2.30	2.25	2.30	2.50	1.91	1.42	1.34
Er	3.89	3.91	3.74	6.99	6.17	6.34	7.15	5.95	3.74	3.70
Tm	0.59	0.57	0.55	1.01	0.95	0.97	1.05	0.85	0.59	0.57
Yb	3.88	3.78	3.58	6.72	6.05	6.10	6.59	5.19	3.66	3.47
Lu	0.58	0.57	0.56	0.97	0.90	0.89	0.95	0.80	0.57	0.57
T zr. sat.	812	834	819	842	839	817	814	817	831	822
Visc. (H_2O = 0%)	10.37	9.74	10.02	9.90	10.30	10.62	10.78	11.57	9.56	9.96
Visc. (H_2O = 1%)	7.38	6.97	7.17	7.33	7.62	7.87	7.99	8.64	6.86	7.21
Visc. (H_2O = 2%)	6.35	6.00	6.17	6.32	6.57	6.79	6.90	7.49	5.89	6.19
Visc. (H_2O = 3%)	5.68	5.36	5.52	5.62	5.85	6.05	6.15	6.70	5.24	5.52
Visc. (H_2O = 4%)	5.16	4.87	5.02	5.08	5.28	5.48	5.57	6.09	4.74	4.99
Tg (H_2O = 0%)	997	995	994	1015	1037	1031	1033	1072	987	997
Tg (H_2O = 1%)	841	839	839	848	866	862	864	901	828	835
Tg (H_2O = 2%)	775	773	773	770	787	783	785	820	759	763
Tg (H_2O = 3%)	729	727	727	714	729	725	728	760	711	713
Tg (H_2O = 4%)	692	691	691	670	683	679	681	712	673	673

IG: Iriri Group; RDIS: Rio Dourado Intrusive Suite; RD: rhyodacite; PMZ: porphyritic monzogranite; FRI: foliated rhyolite; MRI: massive rhyolite; T zr. sat.: the temperature of zircon saturation (°C); Visc.: viscosity (log η Pa s); Tg: glass transition temperature (°C).

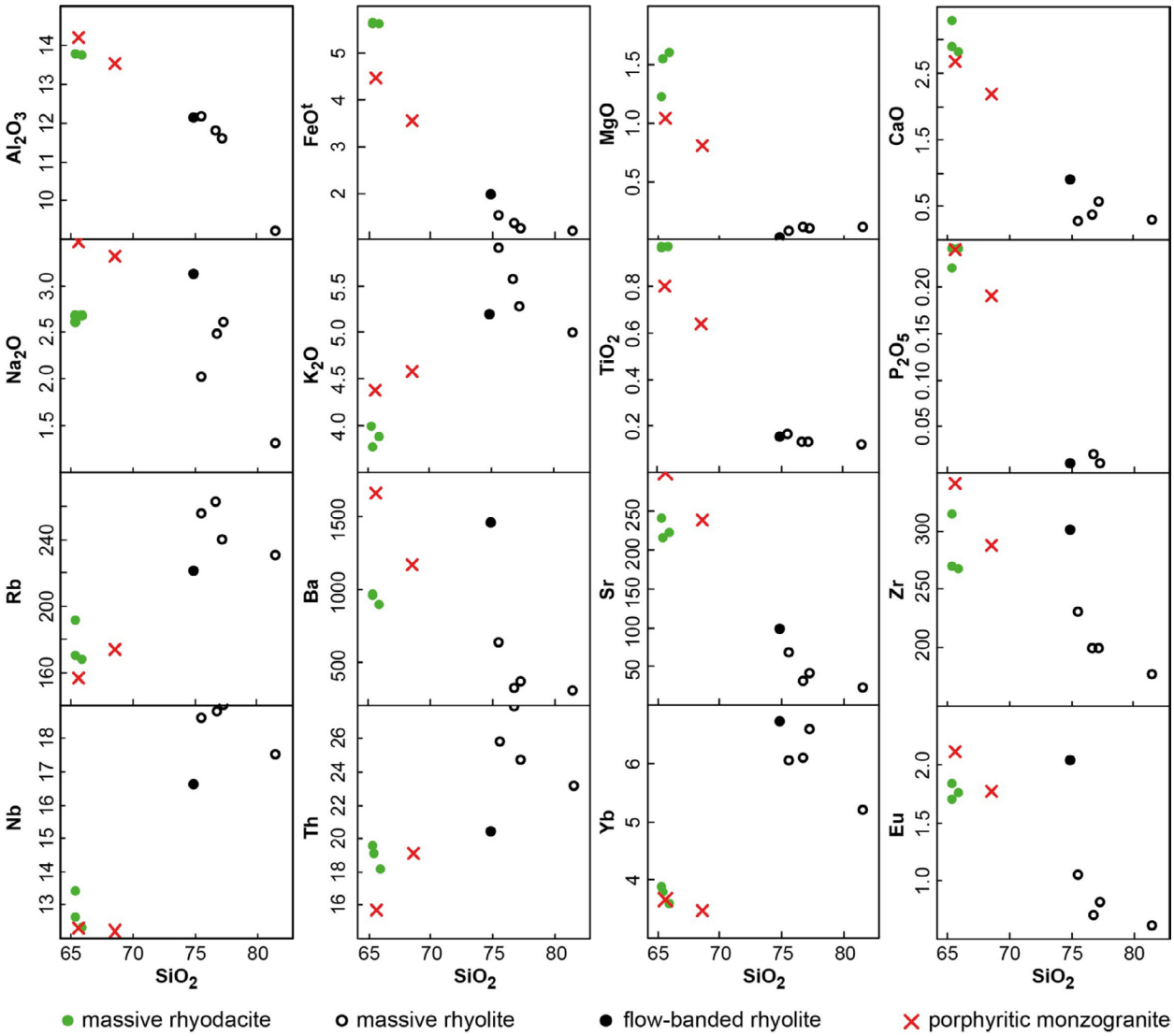

Figure 8. Binary diagrams of the volcanic rocks of the Iriri Group and granitoids of the Rio Dourado Intrusive Suite in the Serra dos Magalhães region.

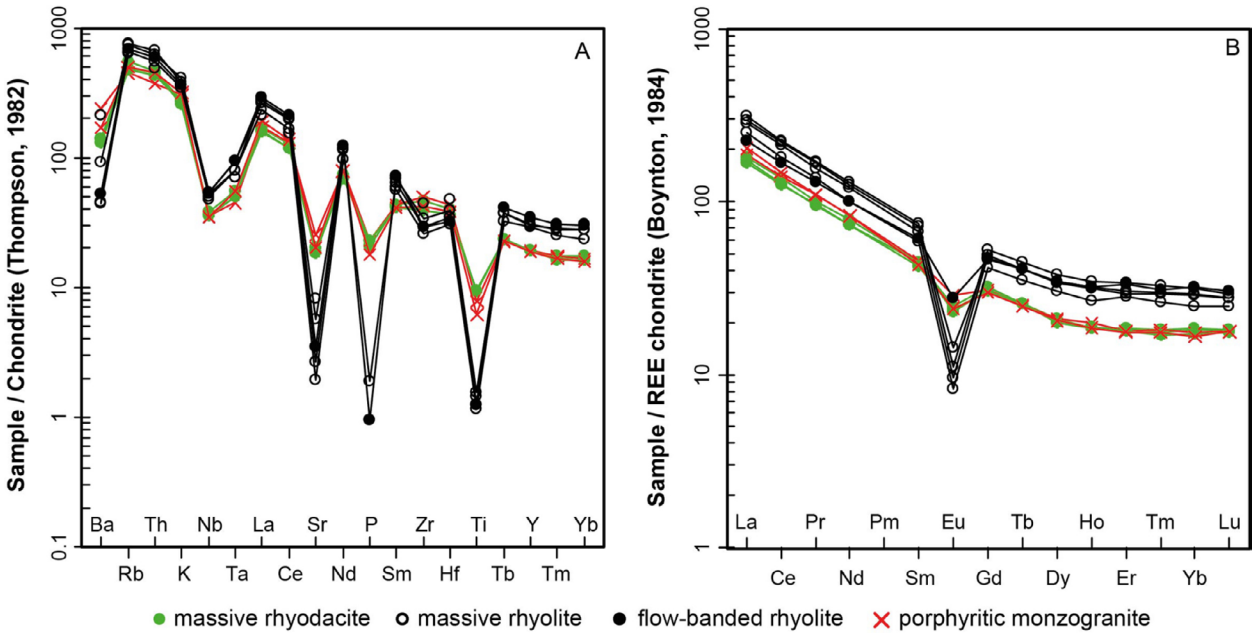

Figure 9. Spidergrams of the volcanic rocks of the Iriri Group and granitoids of the Rio Dourado Intrusive Suite in the Serra dos Magalhães region. (A) Normalized to the Thompson (1982) chondrite pattern. (B) Normalized to the Boynton (1984) chondrite pattern.

the massive rhyolites, moderate in flow-banded rhyolite and slight in massive rhyodacites and porphyritic monzogranites. Both spidergrams evidence the strict similarity between the massive rhyodacites and the porphyritic monzogranites and the lack of transitional features from these lithotypes to the rhyolites (Fig. 9B).

The geochemical classification of volcanic rocks, mainly based on immobile major and trace elements, corroborates the petrographic individualization of rhyodacites and rhyolites and indicates the corresponding field of the granitoids to the porphyritic monzogranite (Figs. 10A and 10B). The diagrams by Frost *et al.* (2001) point out to the metaluminous character of the porphyritic monzogranites and the flow-banded rhyolite, the metaluminous to the slightly peraluminous signature of the massive rhyodacites and the slightly peraluminous of the massive rhyolites (Fig. 10C). Moreover, the diagram of Figure 10D shows the affinity of all lithotypes with the ferroan magmas, since the geochemical terminology of granitoid applies to silicic volcanic rocks. Ferroan magmas usually present strict correlation to the A-type granites (or silicic volcanic rocks) of Loiselle and Wones (1979) as the Whalen *et al.* (1987) diagrams demonstrate (Figs. 11A and 11B). The Eby (1992) division of A-type granites indicates that all studied lithotypes correspond to magmas of A2-type signature (Fig. 11C). Eby (1992) discusses that the A2-type granites can represent magmas that originate from partial remelting of the lithosphere that has undergone a previous melting process or forms partial melting of continental crust.

RHEOLOGY OF VOLCANIC ROCKS

Rheological information from geochemical data were obtained through the Hanchar and Watson (2003) and Giordano *et al.* (2008) models (see section Materials and Methods for details) and allows meaningful interpretation concerning the emplacement of volcanic rocks. Zircon saturation temperature approximates the magma liquidus temperature since zircon is usually an early mineral to crystallize in the magma history. Massive rhyodacites present a mean zircon saturation temperature of 800°C, lower than the rhyolites average (831°C).

The viscosity calculation of each rock considers the assumed magma liquidus temperatures to estimate the viscosity data in dry and wet (1 to 4% of H_2O) conditions. Viscosity in the

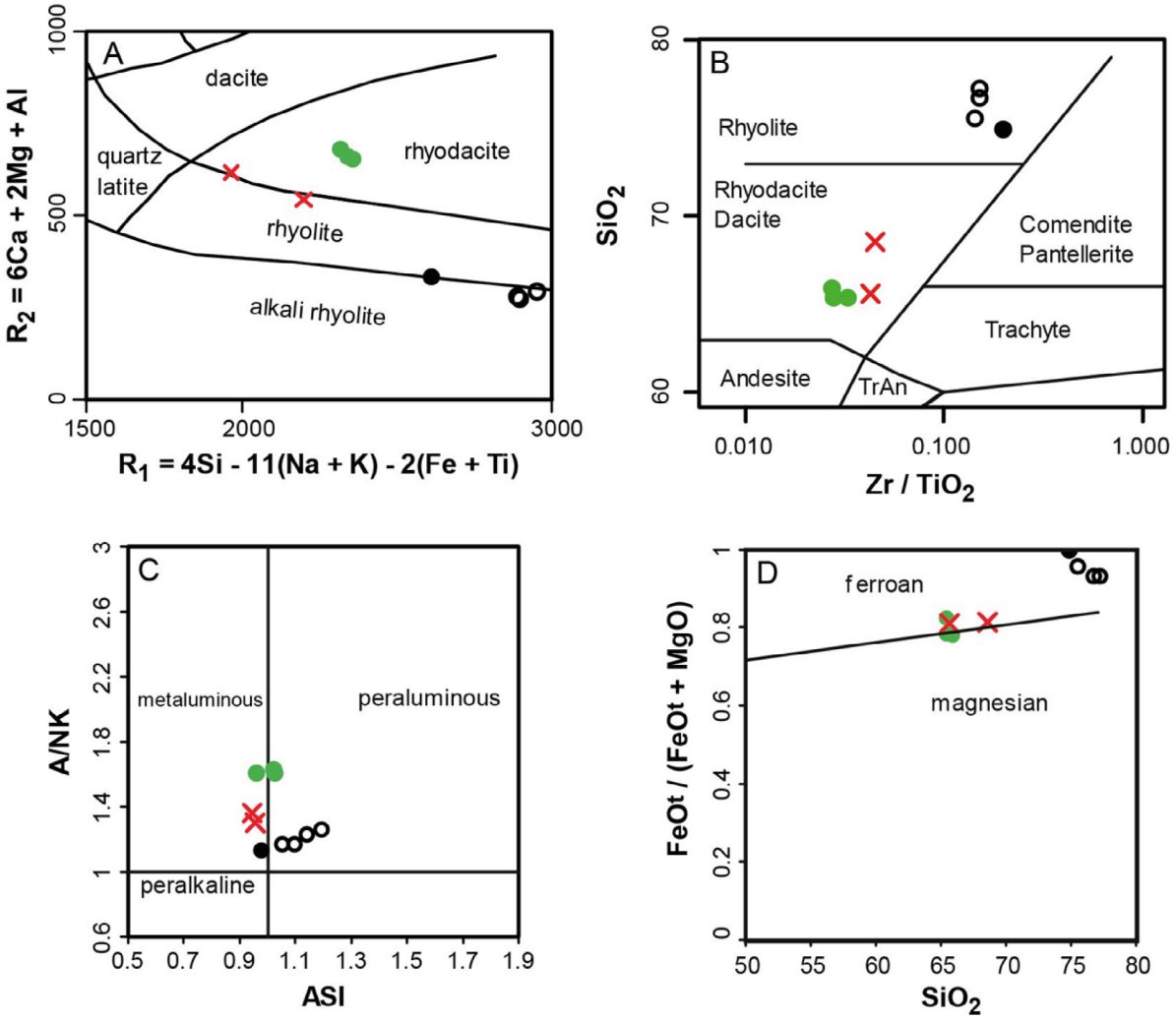

Figure 10. Classificatory diagrams of the volcanic rocks of the Iriri Group and granitoids of the Rio Dourado Intrusive Suite in the Serra dos Magalhães region. (A) La Roche *et al.* (1980). (B) Winchester and Floyd (1977). (C and D) Frost *et al.* (2001).

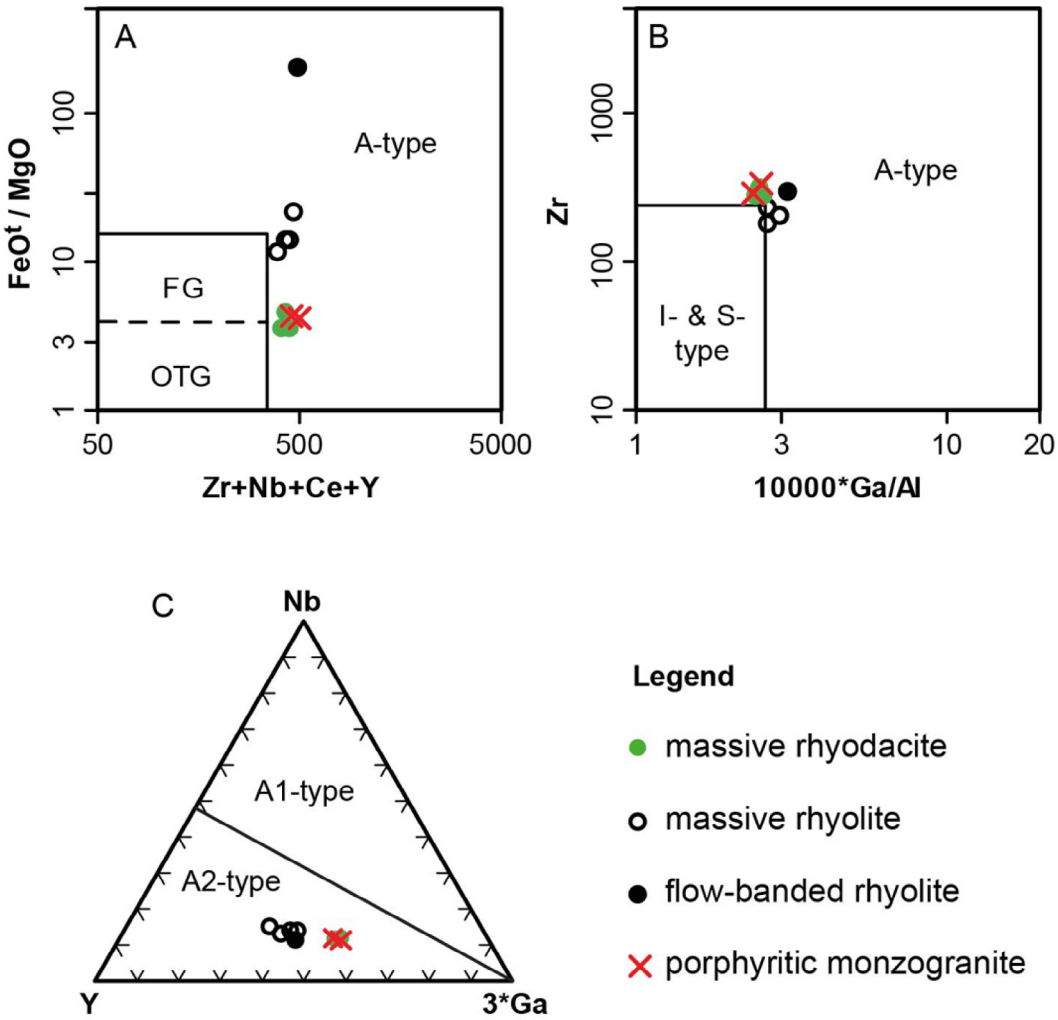

Figure 11. Granite typology diagrams of the volcanic rocks of the Iriri Group and granitoids of the Rio Dourado Intrusive Suite in the Serra dos Magalhães region. (A and B) Whalen *et al.* (1987). (C) Eby (1992).

dry condition is lower in the massive rhyodacites and the flow-banded rhyolite, from 9.74 to 10.37 log η Pa s and of 9.90 log η Pa s, respectively. The massive rhyolites show higher values that range from 10.30 to 11.57 log η Pa s. The increase in H_2O estimation exponentially decreases viscosity, down to around 5.00 log η Pa s in massive rhyodacites and flow-banded rhyolite, and from 5.28 to 6.09 log η Pa s in massive rhyolites (Figs. 12A and 12B).

Estimated glass transition temperatures in dry conditions are of around 995°C in massive rhyodacites, 1,015°C in flow-banded rhyolite, and range from 1,037 to 1,072°C in massive rhyolites. Similarly, the glass transition temperatures exponentially decrease with the H_2O input (Figs. 12C and 12D). However, the reduction is more effective in the rhyolites — down to 670°C in flow-banded rhyolites and around 685°C in massive ones — than in the massive rhyodacites (~690°C).

U-PB GEOCHRONOLOGY

The U-Pb zircon isotopic data of samples DI10a (massive rhyodacite — Iriri Group), DI04a (massive rhyolite — Iriri Group), and DI17a (porphyritic monzogranite — Rio Dourado Intrusive Suite) are available in Table 2.

The results of 9 grains of the DI-010a sample show Th/U ratios ranging from 0.49 to 1.38 and low common Pb contents that vary from 0.04 to 0.44%. The geochronological calculation allows the determination of a concordia age at 2σ of 1870 ± 11 Ma, representing the crystallization age of the massive rhyodacites. Mean-squared weighted deviates (MSWD) of concordance is 0.063 (Fig. 13).

Zircon grains of the DI17a sample are euhedral to subhedral with rare fragmented terminations. The size ranges from 110 to 220 µm and the internal structure show translucent crystals with prominent internal oscillatory zoning and rare inherited cores. The common Pb contents of 21 grains are low and vary from 0.13 to 1.05%. These zircon grains also present low to high Th/U ratios, from 0.52 to 1.69. Most apparent ages are strongly concordant and allow the statistical calculation of an intercept at 1879 ± 5 Ma at 2σ, which represents the crystallization age of the porphyritic monzogranites. MSWD of concordance is 0.78 (Fig. 14).

Zircon grains of the DI14a sample are euhedral to subhedral with frequent fragmented terminations and size from 90 to 150 µm. The internal structure reveals a frequent oscillatory zoning and rare inherited cores. Most of the grains are metamict. Crystals sizes are from 90 to 150 µm, Th/U ratios

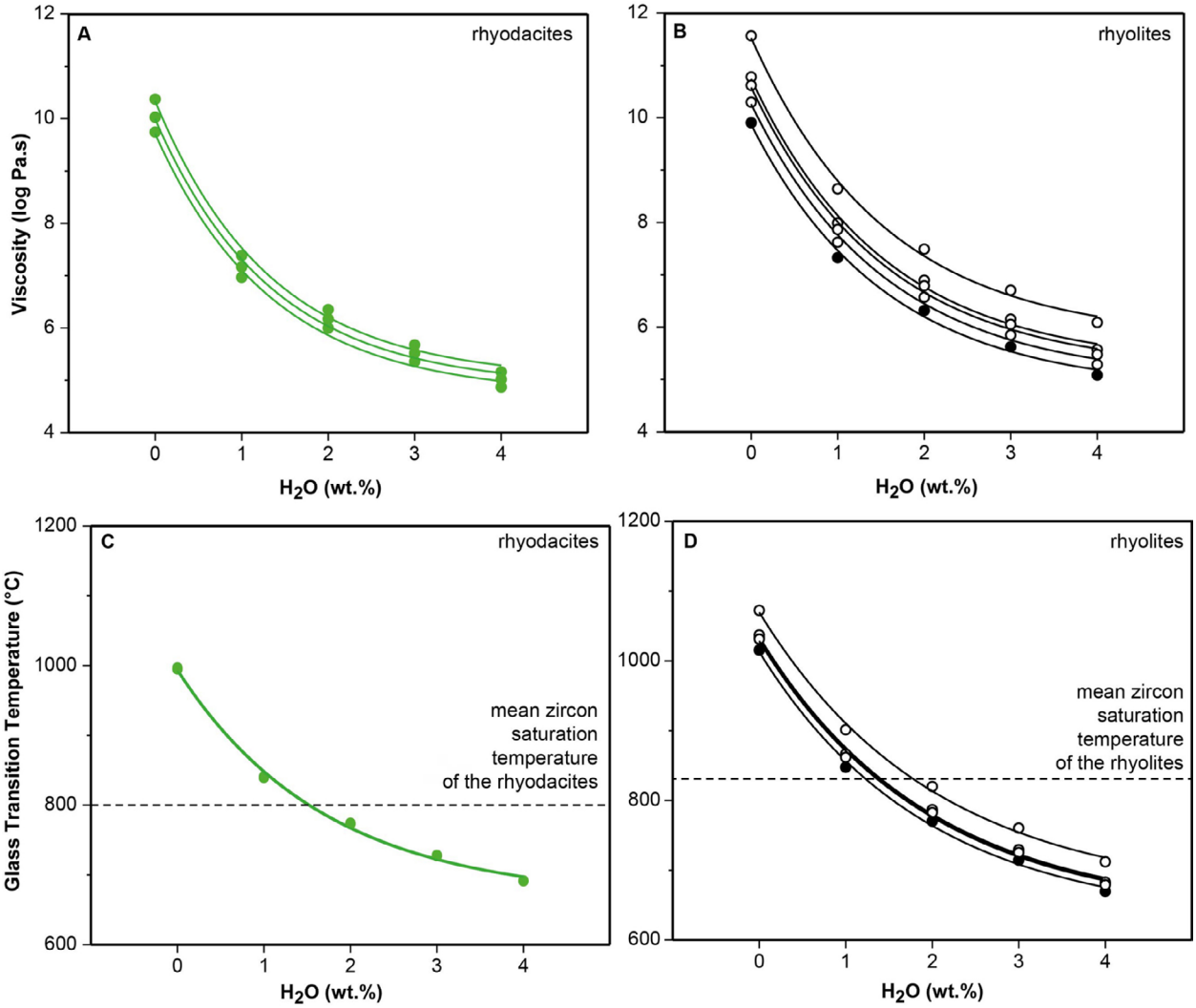

Figure 12. Rheological characteristics of the volcanic rocks of the Iriri Group and granitoids of the Rio Dourado Intrusive Suite in the Serra dos Magalhães region. (A and B) viscosity estimations. (C and D) Glass transition temperature estimations.

Table 2. U-Pb zircon isotopic data of the volcanic and granitic rocks of the Serra dos Magalhães region.

Massive rhyodacite (sample DI10a)														
Spot	U (ppm)	Th (ppm)	Th/U	^{206}Pb (%)	$^{207}Pb/^{235}U$	1 σ (%)	$^{206}Pb/^{238}U$	1 σ (%)	Corr.	Apparent Ages (Ma)				Disc. (%)
										$^{206}Pb/^{238}U$	1 σ	$^{207}Pb/^{206}Pb$	1 σ	
6-1	105	84	0.794	0.04	5.42	2.5	0.338	2.4	0.79	1878	39	1898	28	-2
3-1	99	57	0.580	0.10	5.44	2.5	0.334	2.4	0.72	1856	39	1929	33	+1
6-3	120	103	0.859	0.31	5.71	2.5	0.351	2.5	0.79	1939	42	1926	30	-4
6-4	248	121	0.487	0.14	5.33	2.0	0.339	2.1	0.87	1884	34	1863	19	-1
7-1	115	85	0.735	0.44	5.32	2.4	0.330	2.4	0.79	1837	38	1909	28	+2
7-2	92	69	0.756	0.25	5.36	2.5	0.335	2.5	0.78	1861	40	1896	30	+1
7-3	91	86	0.946	0.25	5.39	4.2	0.343	3.4	0.69	1903	55	1862	56	-2
1-1	356	219	0.616	0.10	5.32	1.9	0.336	2.0	0.83	1870	33	1875	21	+1
10-1	180	248	1.379	0.25	5.67	3.5	0.351	2.5	0.74	1939	42	1914	42	-4
Massive rhyolite (sample DI14a)														
Spot	U (ppm)	Th (ppm)	Th/U	^{206}Pb (%)	$^{207}Pb/^{235}U$	1 σ (%)	$^{206}Pb/^{238}U$	1 σ (%)	Corr.	Apparent Ages (Ma)				Disc. (%)
										$^{206}Pb/^{238}U$	1 σ	$^{207}Pb/^{206}Pb$	1 σ	
2.1	126	70	0.55	0.18	5.229	0.105	0.333	0.003	0.38	1851	0.014	1864	0.036	-1
14.1	115	58	0.51	0.68	5.417	0.119	0.344	0.003	0.59	1908	0.015	1866	0.042	+2
9.1	256	129	0.51	0.11	5.372	0.091	0.342	0.003	0.52	1899	0.013	1860	0.029	+2

Continue...

Table 2. Continuation.

Massive rhyolite (sample DI14a)														
Spot	U (ppm)	Th (ppm)	Th/U	^{206}Pb (%)	$^{207}Pb/^{235}U$	1 σ (%)	$^{206}Pb/^{238}U$	1 σ (%)	Corr.	Apparent Ages (Ma)				Disc. (%)
										$^{206}Pb/^{238}U$	1 σ	$^{207}Pb/^{206}Pb$	1 σ	
20.1	270	130	0.48	0.23	5.478	0.103	0.346	0.003	0.93	1917	0.013	1875	0.035	+2
12.1	214	96	0.45	0.17	5.344	0.092	0.342	0.003	0.63	1897	0.013	1852	0.030	+2
6.1	120	90	0.75	0.29	5.419	0.107	0.346	0.003	0.28	1916	0.015	1857	0.036	+3
11.1	218	120	0.55	0.14	5.454	0.095	0.349	0.003	0.96	1932	0.013	1851	0.030	+4
4.1	309	136	0.44	0.23	5.596	0.094	0.358	0.003	0.72	1971	0.013	1856	0.029	+6
18.1	221	163	0.74	0.08	5.652	0.106	0.362	0.003	0.95	1990	0.013	1854	0.034	+7
10.1	261	142	0.54	1.08	5.673	0.099	0.362	0.003	0.84	1993	0.014	1857	0.030	+7
8.1	206	138	0.67	0.65	5.699	0.101	0.363	0.003	0.95	1999	0.014	1860	0.031	+7
Porphyritic monzogranite (sample DI17a)														
Spot	U (ppm)	Th (ppm)	Th/U	^{206}Pb (%)	$^{207}Pb/^{235}U$	1 σ (%)	$^{206}Pb/^{238}U$	1 σ (%)	Corr.	Apparent Ages (Ma)				Disc. (%)
										$^{206}Pb/^{238}U$	1 σ	$^{207}Pb/^{206}Pb$	1 σ	
25.1	132	95	0.72	0.36	4.930	0.100	0.313	0.003	0.950	1755	0.014	1868	0.035	-7
3.1	91	71	0.78	1.05	5.284	0.117	0.329	0.004	0.970	1834	0.020	1902	0.047	-4
4.1	94	105	1.12	0.31	5.220	0.121	0.327	0.004	0.730	1825	0.020	1890	0.049	-4
6.1	84	92	1.10	0.41	5.269	0.122	0.333	0.004	0.130	1851	0.020	1878	0.049	-2
10.1	69	65	0.94	0.40	5.290	0.126	0.333	0.004	0.210	1854	0.021	1882	0.051	-2
7.1	80	73	0.91	0.47	5.308	0.122	0.334	0.004	0.430	1858	0.020	1884	0.049	-2
2.1	85	82	0.97	0.15	5.407	0.126	0.338	0.004	0.810	1876	0.021	1897	0.048	-2
22.2	146	189	1.30	1.04	5.291	0.102	0.335	0.003	0.680	1861	0.015	1875	0.033	-1
20.1	102	106	1.04	0.59	5.285	0.110	0.335	0.003	0.910	1863	0.016	1870	0.037	-1
5.1	29	48	1.69	0.46	5.411	0.170	0.339	0.005	0.740	1880	0.025	1894	0.069	-1
13.1	76	70	0.92	0.31	5.314	0.127	0.337	0.004	0.750	1871	0.021	1871	0.051	0
17.1	102	96	0.94	0.31	5.350	0.112	0.339	0.003	0.790	1880	0.016	1874	0.036	0
1.1	112	120	1.07	0.15	5.469	0.121	0.342	0.004	0.940	1897	0.020	1894	0.046	0
11.1	67	63	0.94	0.20	5.462	0.135	0.343	0.005	0.820	1903	0.022	1886	0.053	0
24.1	119	96	0.81	0.52	5.333	0.099	0.340	0.003	0.890	1887	0.014	1860	0.034	+1
16.1	213	218	1.02	0.25	5.398	0.097	0.342	0.003	0.910	1894	0.014	1874	0.031	+1
21.1	111	58	0.52	0.51	5.402	0.121	0.345	0.004	0.890	1911	0.017	1857	0.041	+2
22.1	124	119	0.96	0.13	5.530	0.109	0.349	0.003	0.930	1932	0.015	1876	0.034	+2
8.1	188	241	1.28	1.00	5.562	0.119	0.351	0.004	0.960	1937	0.020	1881	0.045	+2
12.1	111	95	0.86	0.23	5.562	0.120	0.354	0.004	0.780	1952	0.020	1865	0.047	+4
18.1	190	197	1.03	0.73	5.738	0.106	0.363	0.003	0.940	1995	0.015	1876	0.032	+6

Corr.: correction; Disc.: discordance.

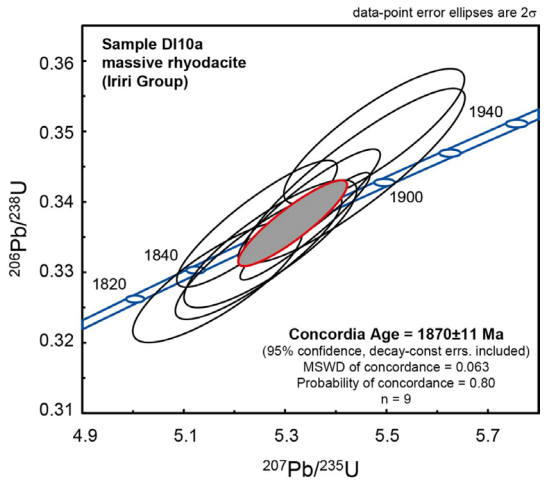

Figure 13. Concordia diagram of the crystallization age of the massive rhyodacite of the Iriri Group (sample DI10a).

and common Pb contents are low and range from 0.44 to 0.75 and 0.08 to 1.08%, respectively. Most of the zircon grains are positively discordant due to the relative uranium gain during the metamictization process. According to Andersen *et al.* (2019) and references therein, redistribution of uranium and lead within zircon grains can occur in crystals that undergone radiation damage, as metamictization, mainly under tropical weathering. Statistical regression yields an intercept at 1863 ± 14 Ma at 2σ, interpreted as crystallization age of the rhyolites. MSWD of concordance is 0.38 (Fig. 15).

The main internal characteristic of the zircon crystals of all samples is the prominent oscillatory zoning. Corfu *et al.* (2003) point out that the well-developed growth zoning is the more typical feature of magmatic zircon. Moreover, the low to high Th/U ratios are also characteristic of zircon grains of igneous origin (Belousova *et al.* 2002, Kirkland *et al.* 2015).

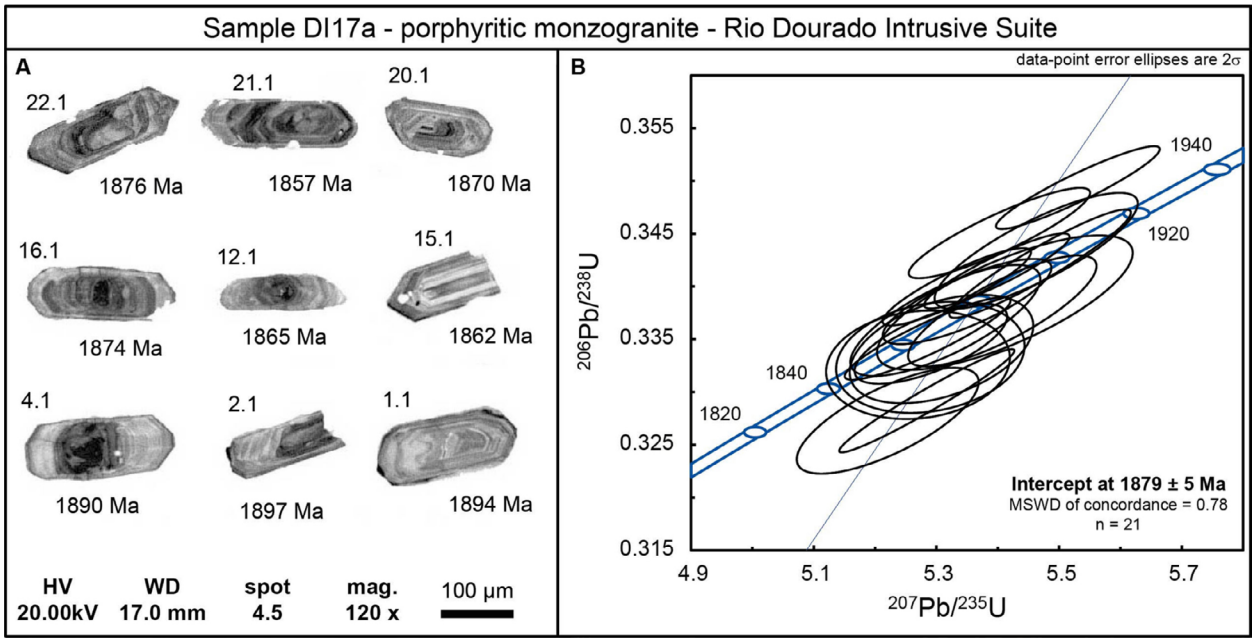

Figure 14. Geochronological illustrations of the massive rhyolite of the Iriri Group (sample DI14a). (A) Cathodoluminescence images of zircon crystals. (B) concordia diagram of the crystallization age.

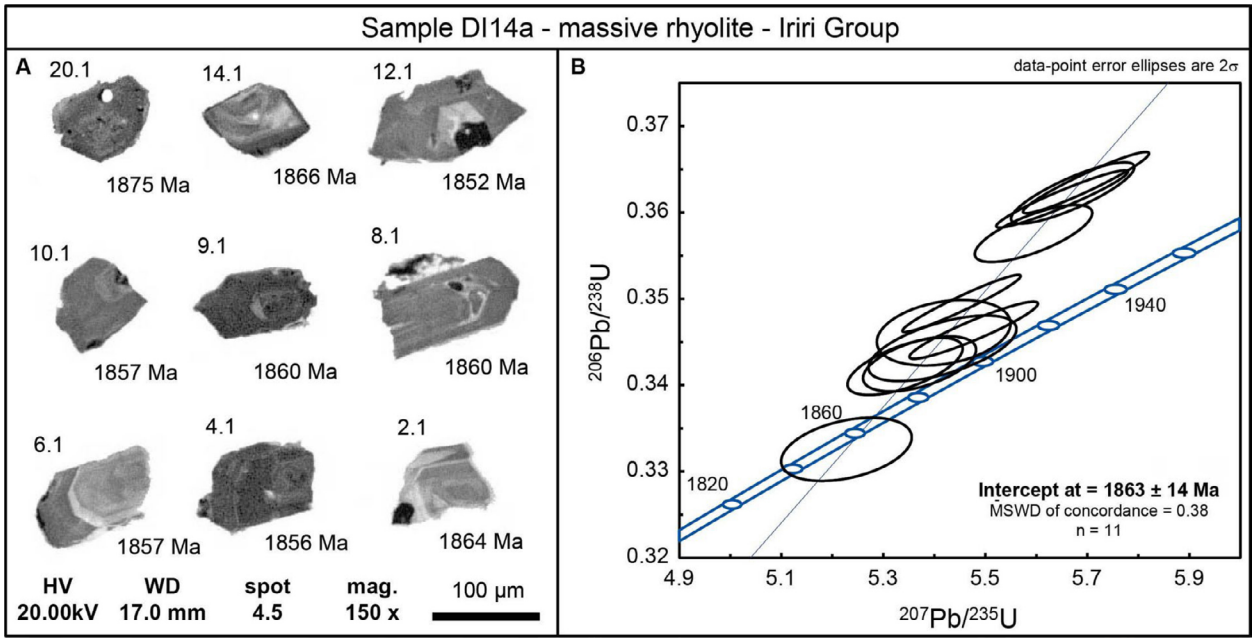

Figure 15. Geochronological illustrations of the porphyritic monzogranite of the Rio Dourado Intrusive Suite (sample DI17a). (A) Cathodoluminescence images of zircon crystals. (B) concordia diagram of the crystallization age.

DISCUSSION

Petrology

The volcanic rocks of the Serra dos Magalhães region present porphyritic texture with dominantly subhedral to euhedral phenocrysts with common embayments and subordinate crystals fragments. The amount of phenocryst fragments in volcanic rocks, as pointed out by Allen and McPhie (2003), may indicate the eruption nature. These authors suggest that the fragmentation of phenocrysts occurs along zones of internal weakness created by the expansion of melt inclusions due to the increased internal pressure caused by decompression during ascent. Moreover, these authors assume that the amount of feldspars and quartz fragments rarely exceed 12% in lavas, even in those with phenocrysts content of up to 28 modal%. The groundmass is holocrystalline aphanitic to hypocrystalline with abundant microlites and crystallites. Lithic and glassy fragments are absent. These features, as presented in Figures 4, 5 and 6, corroborate to the effusive nature of the original eruptions that generated the rhyodacitic and rhyolitic lava flows of the Serra dos Magalhães region.

The subhedral alkali-feldspar megacrysts with abundant xenomorphic quartz inclusions in the porphyritic monzogranites, allied to the xenomorphic quartz crystals of the

medium-grained matrix, as presented in Figure 7, suggest a late stage of crystallization for both phases. The common subhedral to euhedral alkali-feldspar crystals of the matrix indicate the presence of several nuclei during the early stage of crystallization, attesting high nucleation (N) rates of the alkali-feldspar. Reduced nucleation rate and elevated growth rate (G) at a low degree of undercooling at the early stage of crystallization do not properly explain the origin of this feature, as suggested by Swanson (1977) and expected for porphyritic volcanic and subvolcanic systems. Higgins (1999) assumes the presence of alkali-feldspar megacrysts as the result of textural coarsening (or Ostwald ripening) of small and early formed crystals during a late magmatic stage of the pluton crystallization. According to the author, the undercooling buffers near the liquidus of the alkali-feldspar for a long period so that the texture becomes coarsened.

The geochemical signature of the volcanic rocks indicates an intrinsic relation of the massive rhyodacites to the porphyritic monzogranites, with similar contents of major, minor, and trace elements (Fig. 9A), including REE (Fig. 9B). Differently, the geochemical character of massive and flow-banded rhyolites contrasts with the other lithotypes and shows an evolved pattern with higher incompatible elements and high rare earth elements (HREE) content. Binary diagrams show a distribution pattern of distinct poles and no curvilinear correlation among the different rocks. These characteristics suggest a magmatic origin of different batches of melt from a single magmatic source, due to the intrinsically similar geochemical features, whose rhyodacites and monzogranites slightly predated the rhyolites.

Rheological information of the volcanic rocks of the Serra dos Magalhães region indicates high liquidus temperature, usually > 800°C, high viscosity, and glass transition temperature at dry conditions, which both significantly decreased with the water increment. According to Dingwell and Webb (1990), the glass transition of a silicate melt is the phenomenon that marks a shift of the magma dynamics from a crystal-like to a liquid-like behavior. This propriety is temperature-dependent and indicates that above the glass transition temperature the dynamics of a silicate melt are of a true liquid (viscous system), whereas below the glass transition temperature the melt dynamics are solid (elastic system). The model of Giordano *et al.* (2008) demonstrates that the glass transition temperature is also H_2O-dependent. This dynamic behavior of silicate melts, defined by the glass transition, is fundamental to the understanding of eruptional processes, where a viscous system (*i.e.*, liquid behavior) favors an effusive eruption, and an elastic system (*i.e.*, solid behavior) supports a pyroclastic eruption. Rhyodacites and rhyolites of the Serra dos Magalhães region are effusive volcanic rocks formed by subaerial lava flows. The calculated glass transition temperature and its variation with H_2O allow interpreting the dynamics of the magmatic flow of rhyodacites and rhyolites. Assuming the zircon saturation temperature as the true magma temperature of rhyodacites and rhyolites and comparing the variation of the calculated glass transition temperature with the water increment (Figs. 12C and 12D), it is possible to suggest that the rhyodacite and rhyolite magma hosted H_2O content as high as 1.5 and 1.8 wt. %, respectively. Water content higher than these values decrease the viscosity (Figs. 12A and 12B) and the glass transition temperature of rhyodacites and rhyolites below the magma temperature and thus attribute a viscous behavior (*i.e.*, lava flow) rather than an elastic one that favors pyroclastic eruption.

Geotectonic implications

Several authors present interpretations of the geotectonic setting of Uatumã Magmatism emplacement. In the Pitinga and Presidente Figueiredo region, the tectonic setting of the volcano-plutonism of the Uatumã Magmatism is interpreted as related to the post-collisional setting (Valério *et al.* 2009, Ferron *et al.* 2010, Pierosan *et al.* 2011). In the Tapajós Mineral Province, Lamarão *et al.* (2002) relate the tectonic setting of the Uatumã Magmatism to an intracontinental taphrogenetic event, similarly to the initial assumptions of Dall'Agnol *et al.* (1994) to the extensive magmatism in the Central Amazonian Province and of Dall'Agnol *et al.* (1999) to the granitoids of the Carajás Mineral Province region. On the other hand, Cassini *et al.* (2020) assume that the first pulses of the Iriri Group in the Tapajós Mineral Province are synchronous with the Parauari Intrusive Suite relate to slab break off processes that promote astenospheric upwelling, followed by the emplacement of the Maloquinha Intrusive Suite and Iriri volcanic rocks in an early-anorogenic setting.

Fernandes *et al.* (2006, 2011), in the São Félix do Xingu region, indicate that the Iriri Group volcanic rocks and related granitoids emplaced through the transition from the latest stage of an Andean-type subduction event to the earliest stage of a dominantly extensional setting of a continental rift. In the southeastern of the Amazonian Craton, Rocha *et al.* (2012) indicate that the tectonic setting of the Iriri Group relates to the melting of lithospheric mantle previously modified by subduction events. Barros *et al.* (2008) interpret the tectonic setting of the Rio Dourado Intrusive Suite emplacement, as well as the associated felsic volcanism of the Iriri Group, as related to a post-collisional to anorogenic setting.

Petrographic, geochemical, and geochronological information of the volcanic and granitic rocks of the Serra dos Magalhães region indicate a lithostratigraphic correlation to the units of the Amazonian Craton, as the Iriri Group and the Rio Dourado Intrusive Suite, respectively. Since Cenozoic and recent alluvial deposits partially cover the Paleoproterozoic volcanic and granitic rocks occurrences, the area represents an inlier of the Amazonian Craton and implies in the presence of a Paleoproterozoic (or Archean) basement underlying parts of the Bananal Basin. Regional lineaments, mainly identified from satellite images and geophysical investigations, like those presented by Bahia *et al.* (2007) and Faria (2015), suggest that the eastern edge of the Amazonian Craton extends as far as the NNW Tucurui Fault in the Araguaia River. Similarly, the Amazonian Craton southern edge underlies most of the north-eastern part of the Parecis Basin and prolongs up to the lineaments that limit the Brasnorte High and the Pimenta Bueno Graben (Fig. 16).

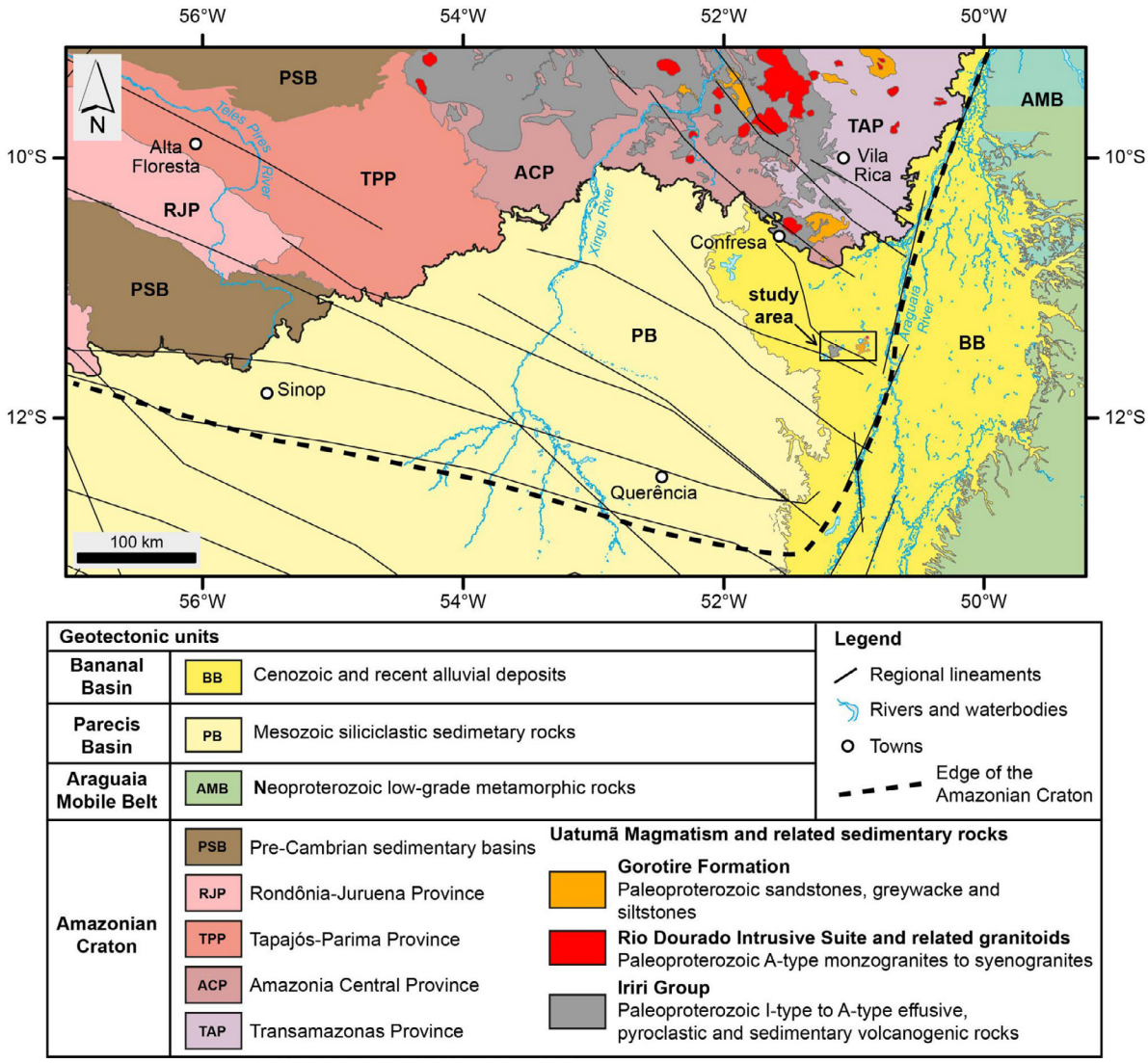

Source: adapted from Lacerda Filho *et al.* (2004), Faraco *et al.* (2004) and Vasquez *et al.* (2008).

Figure 16. Sketch map of the central-southern and southeastern portion of the Amazonian Craton and adjacent geotectonic units.

CONCLUSIONS

Petrologic features of the three volcanic lithotypes indicate at least three eruptive events of effusive character: a less evolved and moderately crystallized (massive rhyodacites) and two evolved and poorly crystallized (massive rhyolites and flow-banded rhyolites). The intrusive event that generates the porphyritic monzogranite underwent a particular crystallization history with typical N/G rate at low to medium undercooling, during its initial stage, and an increasing undercooling at its late stage, promoting the textural coarsening of alkali-feldspar megacrysts. Rhyodacites and monzogranites strongly correlate with one another in terms of geochemical data and show a less evolved ferroan A2-type signature. Geochronological data of these two units present similar crystallization ages. Flow-banded rhyolites share some geochemical similarity to the rhyodacites and monzogranites. The geochemical affinity of massive rhyolites fits a more evolved ferroan A2-type and the crystallization age is slightly younger than the rhyodacites and monzogranites. All lithotypes are comagmatic and contemporaneous and evolved from distinct batches of magma from a single stratified magma chamber.

These Paleoproterozoic volcanic and granitic rocks outcrop amid alluvial deposits, correlate to the known occurrences of the volcano-plutonic association of the Uatumã Magmatism, and point out to the existence of a Paleoproterozoic or Archean basement underlying the Cenozoic sedimentary deposits. This implies the extension of the Amazonian Craton to south-eastern of the assumed region, underlying significant parts of the Parecis and Bananal basins.

ACKNOWLEDGMENTS

This work was supported by *Universidade Federal do Mato Grosso* (UFMT), as field logistic support and sample and thin section preparation, and by the National Council of Scientific and Technological Development (CNPq — project No. 481327/2013-4), for financial support. The personal grants of I.F. Lima and D.I.A. Okuno were supported by the Coordination of Superior Level Staff Improvement (CAPES) and by the PROPeq/UFMT, respectively. Authors also thank the meaningful contributions of the two anonymous reviewers to the improvement of the manuscript.

ARTICLE INFORMATION
Manuscript ID: 20200046. Received on: 06/08/2020. Approved on: 08/28/2020.
I.L. processed and interpreted the geochemical and geochronological data, reinterpreted the thin sections, prepared most of the figures, and wrote the first draft of the manuscript during the master thesis. R.P. was responsible for the feasibility of all data and activities, supervised the first author during the development of the master thesis, and the last author during the undergraduate monography, wrote the final version of the manuscript, and edited the final version of all figures. M.B. developed previous and preliminary research in the study area that motivated this work and made available the location of some outcrops. R.R. contributed to the writing of the "Geotectonic Context" and "Discussion" sections concerning the Parecis Basin. C.S. contributed to the writing of the "Rheology of Volcanic Rocks" section and its implications in the "Discussion" section. D.O. executed the geological mapping and the preliminary thin section interpretation and description during the development of the undergraduate monography.
Competing Interests: The authors declare no competing interests.

REFERENCES

Allen S.R., McPhie J. 2003. Phenocryst fragments in rhyolitic lavas and lava domes. *Journal of Volcanology and Geothermal Research*, **126**(3-4):263-283. https://doi.org/10.1016/S0377-0273(03)00151-3

Alves C.L., Sabóia, A.M., Martins E.G., Stropper J.L. (eds.). 2010. *Geologia e recursos minerais das folhas São José do Xingu SC.22-Y-A e Rio Comandante Fontoura SC.22-Y-B, 1*. Programa de Geologia do Brasil (Projeto noroeste nordeste de Mato Grosso, escala 1:250.000). Goiânia: CPRM, 120 p.

Andersen T., Elburg M.A., Magwaza B.N. 2019. Sources of bias in detrital zircon geochronology: Discordance, concealed lead loss and common lead correction. *Earth-Science Review*, **197**:102899. https://doi.org/10.1016/j.earscirev.2019.102899

Bahia R.B.C., Martins-Neto M.A., Barbosa M.S.C., Pedreira A.J. 2007. Análise da evolução tectonossedimentar da Bacia dos Parecis através de métodos potenciais. *Revista Brasileira de Geociências*, **37**(4):639-649.

Barbosa O., Ramos J.R.A., Gomes F.A., Helmbold R. 1966. *Geologia estratigráfica, estrutural e econômica da área do "Projeto Araguaia"*. Rio de Janeiro: IBGE, 94 p.

Barreto C.J.S., Lafon J.M., Rosa-Costa L.T., Lima E.F. 2014. Palaeoproterozoic (~1.89 Ga) felsic volcanism of the Iricoumé Group, Guyana Shield, South America: geochemical and Sm-Nd isotopic constraints on sources and tectonic environment. *International Geology Review*, **56**(11):1332-1356. https://doi.org/10.1080/00206814.2014.930800

Barros M.A.S., Padilha R.A., Rubert R.R., Silva A.G. D., Pimentel M.M. 2005. Grupo Iriri e Granito Rio Dourado, magmatismo Paleoproterozóico do sul da Área Xingú-Iricoumé –Nordeste de Mato Grosso. *In*: Simpósio de Vulcanismo e Ambientes Associados, 3., 2005, Cabo Frio. *Resumos...*, v. 1, p. 1-6.

Barros M.A.S., Pimentel M.M., Dantas E.L., Padilha R.A. 2008. Geoquímica e Dados Isotópicos das Suítes Intrusivas Vila Rica e Rio Dourado – Mato Grosso – Área Xingu – Província Amazônia Central - Sul do Cráton Amazônico. *In*: Simpósio de Vulcanismo e Ambientes Associados, 4., 2008, Foz do Iguaçu. *Resumos...*, p. 1-4.

Barros M.A.S., Pimentel M.M., Rocha M.L.B.P., Silva F.R., Padilha R.A., Dantas E.L., Moura E. 2011. A Suíte Intrusiva Rio Dourado - Um Granito Tipo A de 1,88 Ga - Sudeste do Craton Amazônico - Mato Grosso – Brasil. *Geologia USP. Série Científica*, **11**(1):75-93. https://doi.org/10.5327/Z1519-874X2011000100005

Barros M.A.S., Rubert R.R., Padilha R.A., Pimentel M.M., Silva G.D. 2006. Dados Preliminares sobre o plutono-vulcanismo do Nordeste de Mato Grosso. *In*: Fernandes C.J., Viana R.R. (Eds.). *Coletânea Geológica do Estado de Mato Grosso*, 1, p. 131-147. Cuiabá: Ed-UFMT.

Belousova E.A., Griffin W.L., O'Reilly S.Y., Fisher N.I. 2002. Igneous zircon: trace element composition as an indicator of source rock type. *Contributions to Mineralogy and Petrology*, **143**:602-622. https://doi.org/10.1007/s00410-002-0364-7

Boynton W.V. 1984. Cosmochemistry of the rare earth elements: meteorite studies. *In*: Henderson P. (Ed.). Rare-earth Elements Geochemistry. *Developments in Geochemistry*, p. 63-114. Amsterdam: Elsevier.

Braga L.G., Pierosan R., Geraldes M.C. 2020. Paleoproterozoic (~2.0 Ga) volcano-plutonism in the southeastern region of the Amazon Craton: Petrological aspects and geotectonic implications. *Geological Journal*, **55**(6):4352-4374. https://doi.org/10.1002/gj.3686

Cassini L.V., Moyen J.F., Juliani C. 2020. Orosirian magmatism in the Tapajós Mineral Province (Amazonian Craton): The missing link to understand the onset of Paleoproterozoic tectonics. *Lithos*, **356-357**:105350. https://doi.org/10.1016/j.lithos.2019.105350

Corfu F., Hanchar J.M., Hoskin P.W.O., Kinny P. 2003. Atlas of zircon textures. *In*: Hanchar J.M., Hoskin P.W.O. (Eds.). Zircon. *Reviews in Mineralogy and Geochemistry*, 53, p. 469-500. Mineralogical Society of America and Geochemical Society.

Corrêa L.W.C., Macambira M.J.B. 2014. Evolução da região de Santana do Araguaia (PA) com base na geologia e geocronologia Pb-Pb em zircão de granitoids. *Geologia USP. Série Científica*, **14**(2):45-66. http://dx.doi.org/10.5327/Z1519-874X201400020003

Costi H.T., Dall'Agnol R., Moura C.A. 2000. Geology and Pb-Pb geochronology of Paleoproterozoic volcanic and granitic rocks of Pitinga Province, Amazonian Craton, northern Brazil. *International Geology Review*, **42**(9):832-849. https://doi.org/10.1080/00206810009465114

Cunha B.C.C., Potiguar L.A.T., Lanhez A.C., Bezerra P.E.L., Pitthan J.H.L., Souza J. 1981. *Projeto RadamBrasil*. Folha SC.22. Tocantins. Rio de Janeiro: DNPM.

Dall'Agnol R., Lafon J.M., Macambira M.J.B. 1994. Proterozoic Anorogenic Magmatism in the Central Amazonian Province, Amazonian Craton: Geochronological, Petrological and Geochemical Aspects. *Mineralogy and Petrology*, **50**:113-138. https://doi.org/10.1007/BF01160143

Dall'Agnol R., Rämö O.T., Magalhães M.S., Macambira M.J.B. 1999. Petrology of the anorogenic, oxidised Jamon and Musa granites, Amazonian Craton: implications for the genesis of Proterozoic A-type granites. *Lithos*, **46**(3):431-462. https://doi.org/10.1016/S0024-4937(98)00077-2

Dingwell D.B., Webb S.L. 1990. Relaxation in silicate melts. *European Journal of Mineralogy*, **2**(4):427-449.

Eby G.N. 1992. Chemical subdivision of the A- type granitoids: petrogenetic and tectonic implication. *Geology*, **20**(7):641-644. https://doi.org/10.1130/0091-7613(1992)020%3C0641:CSOTAT%3E2.3.CO;2

Faraco M.S.G., Bahia R., Oliveira M.A. 2004. Folha SA.21-Santarém. *In*: Schobbenhaus C., Gonçalves J.H. (Eds.). *Carta Geológica do Brasil ao Milionésimo*. Sistemas de Informações Geográficas-SIG. Programa Geologia do Brasil. Brasília: CPRM. CD-ROM.

Faria H.P.A. 2015. *Caracterização de domínios tectono-geofísicos na Bacia dos Parecis com base em dados de métodos potenciais*. MS Dissertation, Instituto de Geociências, Universidade de Brasília, Brasília, 142 p.

Fernandes C.M.D., Juliani C., Monteiro L.V.S., Lagler B., Misas C.M.A. 2011. High-K calc-alkaline to A-type fissure-controlled volcano-plutonism of the São Félix do Xingu region, Amazonian craton, Brazil: Exclusively crustal sources or only mixed Nd model ages? *Journal of South American Earth Sciences*, **32**(4):351-368. https://doi.org/10.1016/j.jsames.2011.03.004

Fernandes C.M.D., Lamarão C.N., Teixeira N.P. 2006. O vulcanismo bimodal do tipo Uatumã da região de São Félix do Xingu (PA), Província Mineral de Carajás. *Revista Brasileira de Geociências*, **36**(3):523-534.

Ferron J.M.T.M., Bastos Neto A.C., Lima E.F., Nardi L.V.S., Costi H.T., Pierosan R., Prado M. 2010. Petrology, geochemistry, and geochronology of Paleoproterozoic volcanic and granitic rocks (1.89–1.88 Ga) of the Pitinga Province, Amazonian Craton, Brazil. *Journal of South American Earth Sciences*, **29**(2):483-497. https://doi.org/10.1016/j.jsames.2009.05.001

Frost B.R., Barnes C.G., Collins W.J., Arculus R.J., Ellis D.J., Frost C.D. 2001. A geochemical classification of granitic rocks. *Journal of Petrology*, **42**(11):2033-2048. https://doi.org/10.1093/petrology/42.11.2033

Giordano D., Russel J.K., Dingwell D.B. 2008. Viscosity of magmatic liquids: a model. *Earth and Planetary Science Letters*, **271**(1-4):123-134. https://doi.org/10.1016/j.epsl.2008.03.038

Hanchar J.M., Watson E.B. 2003. Zircon saturation thermometry. *In*: Hanchar J.M., Hoskin P.W.O. (Eds.). Zircon. *Reviews in Mineralogy and Geochemistry*, 53, p. 89-112. Mineralogical Society of America and Geochemical Society.

Higgins M.D. 1999. Origin of megacrysts in granitoids by textural coarsening: a crystal size distribution (CSD) study of microcline in the Cathedral Peak Granodiorite, Sierra Nevada, California. *In*: Castro A., Fernández C., Vigneresse J.L. (Eds.). *Understanding Granites:* Integrating New and Classical Techniques, 168, p. 207-219. London: Geological Society of London Special Publication.

Jackson S.E., Pearson N.J., Griffin W.L., Belousova E.A. 2004. The application of laser ablation-inductively coupled plasma-mass spectrometry to in situ U–Pb zircon geochronology. *Chemical Geology*, **211**(1-2):47-69. https://doi.org/10.1016/j.chemgeo.2004.06.017

Kirkland C.L., Smithies R.H., Taylor R.J.M., Evans N., McDonald B. 2015. Zircon Th/U ratios in magmatic environs. *Lithos*, **212-215**:397-414. https://doi.org/10.1016/j.lithos.2014.11.021

Klein E.L., Almeida M.E., Rosa-Costa L.T. 2012. *The 1.89-1.87 Ga Uatumã Silicic Large Igneous Province, northern South America*. Available at: <http://www.largeigneousprovinces.org>. Accessed on: July, 2019.

Klein E.L., Almeida M.E., Vasquez M.L., Bahia R.B.C., Santo M.L.E., Ferreira A.L. (Eds.). 2001. *Geologia e Recursos Minerais da Província Mineral do Tapajós:* Folhas: Vila Mamãe Anã (SB.21-V-D), Jacareacanga (SB.21-Y-B), Caracol (SB.21-X-C), Vila Riozinho (SB.21-Z-A) e Rio Novo (SB.21-Z-C). Estados do Pará e Amazonas. Escala 1:500.000. Brasília: CPRM/DIEDIG/DEPAT, 81 p.

La Roche H., Leterrier J., Grandclaude P., Marchal M. 1980. A classification of volcanic and plutonic rocks using R1R2-diagram and major-element analyses – its relationship with current nomenclature. *Chemical Geology*, **29**(1-4):183-210. https://doi.org/10.1016/0009-2541(80)90020-0

Lacerda Filho J.V., Abreu Filho W., Valente C.R., Oliveira C.C., Albuquerque M.C. 2004. *Geologia e recursos minerais do Estado de Mato Grosso:* texto explicativo dos mapas geológico e de recursos minerais do Estado de Mato Grosso. Programa Integração, Atualização e Difusão de Dados da Geologia do Brasil e Subprograma Mapas Geológicos estaduais, escala 1:1.000.000. Cuiabá: MME/CPRM/SICME-MT, 235 p.

Lamarão C.N., Dall'Agnol R., Lafon J.M., Lima E.F. 2002. Geology, geochemistry, and Pb-Pb zircon geochronology of the Paleoproterozoic magmatism of Vila Riozinho, Tapajós Gold Province, Amazonian craton, Brazil. *Precambrian Research*, **119**(1-4):189-223. https://doi.org/10.1016/S0301-9268(02)00123-7

Lamarão C.N., Souza K.S., Dall'Agnol R., Galarza M.A. 2008. Granitos pórfiros da região de vila Riozinho, província aurífera do Tapajós: petrografa e geocronologia. *Revista Brasileira de Geociências*, **38**(3):533-543.

Loiselle M.C., Wones D. R. 1979. Characteristics and origin of anorogenic granites. Geological Society of America. *Geological Society of America, Abstracts with programs*, **11**:468.

Ludwig K.R. 2012. *User's Manual for Isoplot 3.75*. Berkeley: Berkeley Geochronology Center Special Publication, 75 p.

Monteiro P.M., Rolando A.P., Macambira M.J.B. 2004. Proveniência de zircão de quartzitos da Formação Gorotire e Grupo Rio Fresco, Serra do Inajá, sul da Província Mineral do Carajás. *In*: Congresso Brasileiro de Geologia, 42., 2004, Araxá. *Resumos...* v. 1, p. 1-2.

Padilha R.A., Barros M.A.S., Pimentel M.M., Dantas E.L. 2007. Petrografia, geoquímica e geocronologia da Suíte Intrusiva Vila Rica – borda sudeste do Craton Amazonico (Provincia Amazonia Central) – Nordeste Do Estado De Mato Grosso. *In*: Simpósio de Geologia da Amazônia, 10., 2007, Porto Velho. *Resumos...* v. 1, p. 1-4.

Pierosan R., Lima E.F., Nardi L.V.S., Bastos Neto A.C., Campos C.P., Jarvis K., Ferron J.M.T.M., Prado M. 2011. Geochemistry of Palaeoproterozoic volcanic rocks of the Iricoumé Group, Pitinga Mining District, Amazonian craton, Brazil. *International Geology Review*, **53**(8):946-979. https://doi.org/10.1080/00206810903391542

Pinho M.A.S.B., Rubert R.R., Silva G.D., Chemale Jr. F., Dussin I.A., Costa E.C. 2004. Dados Petrográficos, Geoquímicos e idades U-Pb da vulcânica félsica do Grupo Iriri na porção nordeste de Mato Grosso – Serra dos Magalhães. *In*: Congresso Brasileiro de Geologia, 42., 2004. *Resumos...* v. 1, p. 1676-1677.

Reis N.J., Almeida M.E., Riker S.L., Ferreira A.L. 2006. *Geologia e recursos minerais do estado do Amazonas*. Programa Geologia do Brasil (mapas geológicos estaduais, escala 1:1.000.000). Manaus: CIAMA/CPRM, 144 p.

Ribeiro P.S.E., Alves C.L. 2017. *Geologia e recursos minerais das folhas Miracema do Norte SC.22-X-D, Porto Nacional SC.22-Z-B, Santa Teresinha SC.22-Z-A*. Programa Geologia do Brasil (Levantamentos Geológicos Básicos, escala 1:250.000). Goiânia: CPRM, 483 p.

Rocha M.L.B.P., Barros M.A.S., Lima E.F., Pierosan R. 2012. Paleoproterozoic Domo of Lava from Iriri Group – Sonho Meu Farm – Northeast of Mato Grosso, Amazon Craton: geology, geochemistry, and geochronology. *Revista Brasileira de Geociências*, **42**(3):471-488. http://dx.doi.org/10.5327/Z0375-75362012000300003

Rubert R.R., Mizusaki A.M.P., Martinelli A.G. 2019. Mesozoic tectonic in the deposition and evolution of Cretaceous sedimentar packages of the Parecis Basin, center-western Brazil. *Journal of South American Earth Sciences*, **93**:140-154. https://doi.org/10.1016/j.jsames.2019.05.002

Rubert R.R., Mizusaki A.M.P., Martinelli A.G., Urban C. 2017. Paleoenvironmental reconstruction and evolution of an Upper Cretaceous lacustrine-fluvial-deltaic sequence in the Parecis Basin, Brazil. *Journal of South American Earth Sciences*, **80**:512-528. https://doi.org/10.1016/j.jsames.2017.10.013

Santos J.O.S. 2003. Geotectônica dos Escudos das Guianas e Brasil Central. *In*: Bizzi L.A., Schobbenhaus C., Vidotti R.M., Gonçalves J.H. (Eds.). *Geologia, tectônica e recursos minerais do Brasil*. Brasília: CPRM, 198 p.

Santos J.O.S., Groves D.I., Hartmann L.A., Moura M.A., McNaughton N.J. 2001. Gold deposits of the Tapajós and Alta Floresta Domains, Tapajós–Parima orogenic belt, Amazon Craton, Brazil. *Mineralium Deposita*, **36**:278-299.

Santos J.O.S., Hartmann L.A., Gaudette H.E., Groves D.I., Mcnaughton N.J., Fletcher I.R. 2000. A New Understanding of the Provinces of the Amazon Craton Based on Integration of Field Mapping and U-Pb and Sm-Nd Geochronology. *Gondwana Research*, **3**(4):453-488. https://doi.org/10.1016/S1342-937X(05)70755-3

Santos J.O.S., Van Breemen O.B., Groves D.I., Hartmann L.A., Almeida M.E., McNaughton N.J., Fletcher I.R. 2004. Timing and evolution of multiple Paleoproterozoic magmatic arcs in the Tapajós Domain, Amazon Craton: constraints from SHRIMP and TIMS zircon, baddeleyite and titanite U–Pb geochronology. *Precambrian Research*, **131**(1-2):73-109. https://doi.org/10.1016/j.precamres.2004.01.002

Stacey J.S., Kramers J.D. 1975. Approximation of terrestrial lead isotope evolution by a two-stage model. *Earth Planetary Science Letters*, **26**(2):207-221. https://doi.org/10.1016/0012-821X(75)90088-6

Swanson S.E. 1977. Relation of nucleation and crystal-growth rate to the development of granitic textures. *American Mineralogist*, **62**(9-10):966-978.

Tarelow Neto J., Pierosan R., Barros M.A.S., Chemale Jr. F., Santos F.S. 2017. Magmatic microgranular enclaves of the northeast of Mato Grosso, Brazil, SE Amazonian Craton: Insights into the magmatism of the Uatumã Supergroup on the basis of field and petrological data. *Journal of South American Earth Sciences*, **78**:61-80. https://doi.org/10.1016/j.jsames.2017.06.004

Tassinari C.C.G., Macambira M.J. 1999. Geochronological provinces of the Amazonian Craton. *Episodes*, **22**(3):174-182. https://doi.org/10.18814/epiiugs/1999/v22i3/004

Teixeira N.P., Bettencourt J.S., Dall'Agnol R., Moura C.A.V., Fernandes C.M.D., Pinho S.C.C. 2005. Geoquímica dos granitos paleoproterozóicos da Suíte Granítica Velho Guilherme, Província Estanífera do Sul do Pará. *Revista Brasileira de Geociências*, **35**(2):217-226.

Thompson R.N. 1982. Magmatism of the British Tertiary volcanic province. *Scottish Journal of Geology*, **18**:49-107. https://doi.org/10.1144/sjg18010049

Valente C.R. 2007. *Geotectonic, geologic evolution and regional geomorphology of the Araguaia river basin, Central Brazil*. PhD Thesis, Universidade Federal de Goiás, Goiânia, 204 p.

Valério C.S., Souza V.S., Macambira M.J.B. 2009. The 1.90–1.88 Ga magmatism in the southernmost Guyana Shield, Amazonas, Brazil: Geology, geochemistry, zircon geochronology, and tectonic implications. *Journal of South American Earth Sciences*, **28**(3):304-320. https://doi.org/10.1016/j.jsames.2009.04.001

Vasquez M.L., Chaves C.L., Moura E.M., Oliveira J.K.M., Lafon J.M. 2013. Eventos magmáticos de 2020–1980 Ma nas folhas São Domingos e Jardim do Ouro, porção leste do Domínio Tapajós. *In*: Simpósio de Geologia da Amazônia, 13., 2013, Belém. *Resumos*... v. 1, p. 209-212.

Vasquez M.L., Cordani U.G., Sato K., Barbosa J.P.O., Faraco M.T.L., Maurer V.C. 2019. U-Pb SHRIMP dating of basement rocks of the Iriri-Xingu domain, Central Amazonian province, Amazonian Craton, Brazil. *Brazilian Journal of Geology*, **49**(3):e20190067. https://doi.org/10.1590/2317-4889201920190067

Vasquez M.L., Klein E.L., Macambira M.J.B., Santos A., Bahia R.B.C., Ricci P.S.F., Quadros M.L.E.S. 2000. Geochronology of granitoids, mafic intrusions, and mineralizations of the Tapajós Gold Province, Amazonian Craton, Brazil. *In*: International Geological Congress, 31., 2000, Rio de Janeiro. *Resumos*... v. 1, p. 1.

Vasquez M.L., Rosa-Costa L.T. (Eds.). 2008. *Geologia e recursos minerais do Estado do Pará*. Programa Geologia do Brasil (mapas geológicos estaduais, escala 1:1.000.000). Belém: MME/CPRM, 328 p.

Whalen J.B., Currie K.L., Chappell B.W. 1987. A-type granites: geochemical characteristics, discrimination and petrogenesis. *Contributions to Mineralogy and Petrology*, **95**:407-419. https://doi.org/10.1007/BF00402202

Williams I.S. 1998. U-Th-Pb Geochronology by Ion Microprobe. *In*: McKibben M.A., Shanks III W.C., Ridley W.I. (eds.). *Applications of microanalytical techniques to understanding mineralizing processes. Reviews in Economic Geology*. v.7. p. 1-35. https://doi.org/10.5382/Rev.07

Winchester J.A., Floyd P.A. 1977. Geochemical discrimination of different magma series and their differentiation products using immobile elements. *Chemical Geology*, **20**:325-343. https://doi.org/10.1016/0009-2541(77)90057-2